Biomarker evidence for the depositional environment of basinal UK Mississippian mudstones

Michael J. E. Sims, M. A. Sephton, J. S. Watson, A. J. Fraser & C. H. Vane

Biomarker evidence for the depositional environment of basinal UK Mississippian mudstones

Michael J. E. Sims[1*],M. A. Sephton[1], J. S. Watson[1], A. J. Fraser[1], C. H. Vane[2]

[1]Department of Earth Science and Engineering, Imperial College London, South Kensington Campus, SW7 2AZ, UK

[2]British Geological Survey, Keyworth, Nottinghamshire, NG12 5GG, UK

Abstract

The regional character of organic matter type and depositional conditions of Pendleian, Brigantian and Arnsbergian mudstones between the Craven Basin and the Widmerpool Gulf was compared through interpretation of biomarker and pyrolysis data from 201 samples recovered from 9 boreholes. The Carboniferous seaways have been determined to commonly host dysoxic conditions, enabling preservation of a mixture of marine and terrestrial organic matter types. Photic zone anoxia evidenced by aryl-isoprenoids was determined to be persistent during 'marine' conditions represented by marine band, high sea level and carbonate facies. Observation and correlation of diasteranes and T_s/T_m ratios within the samples and to other maturity parameters highlighted a significant clay mineral catalytic and/or hydrocarbon retention effect in the samples. This influenced both biomarkers as well as T_{max} thermal maturity data reducing the reliability of such results in interpreting burial and ultimately reserve potential.

The Carboniferous geology of northern England provides a record of an ancient epicontinental seaway. The lithofacies recorded from the shelf, basin and deltas of the seaway has hosted hydrocarbon, metal and coal resource plays, which in turn has directed industrial endeavours as well as scientific enquiry across northern England (Waters et al 2020a). Inspired by gas in place (GIP) estimates of 822-2,281 tcf (Andrews 2013), the most recent industrial interest was for sources of unconventional gas from shale. The target source rocks were the Bowland Shale and Hodder Mudstone formations. Understanding the controls on organic matter type and its distribution in the prospective rocks has been identified as a key characteristic to determine the potential of unconventional resources (Andrews 2013). Different studies have identified differing controls on the organic matter type. Using programmed pyrolysis data mixed type II/III kerogens have been inferred from comparison of S2 and Total Organic Carbon (TOC) content (Waters et al 2020b; Gross et al 2015). However, studies on kerogen kinetics and palynology have attested to type II and I kerogen generative capability (Newport et al 2020; Yang et al 2016; Hennissen et al 2017). Environmental factors controlling water column stratification, redoxclines and sediment source has been cited as generating variability in the potential of the formations by preferentially preserving organic matter (Emmings et al 2020a; Gross et al 2015), understanding these is vital to detemine Mississippian basinal setting and resources sourced.

The main unconventional target in the Carboniferous succession of northern England is the Bowland Shale Formation, defined as a grouping of the regional formations of the Hollywell, Edale and Bowland Shale formations (Waters et al, 2009). The formation is described as dark grey fissile to blocky hemipelagic mudstones, which transitioned with decreasing age from a calcareous to siliciclastic mineralogy (Waters et al 2009; Clarke et al 2018; Waters et al 2020b). Other relevant formations include the Morridge formations which has been used as analogue studies or alternative targets, despite these formations having a greater siliciclastic content (i.e. Gross et al 2015; Konitzer et al 2014; Hennissen et al 2017; Whitelaw et al 2019; Yang et al 2016; Slowakiewicz et al 2015). Data from Microscale Sealed Vessel (MSSV) pyrolysis on the source rock demonstrated a promising Type II kerogen productive capability (Yang et al 2016). Recent resource estimates derived from High-Pressure Water Pyrolysis on Arnsberian and Pendleian samples have reduced the GIP estimates to 140 ± 55 tcf further limited by a 10 % economic recovery for northern England (Whitelaw et al 2019).The source rock facies were confined primarily within half-graben basins, however deposition extended onto the shelves in association with maximum flooding surfaces (Waters et al 2020b). This was calculated to have occurred in a 110 ka cycle for flooding surfaces with closely related faunal assemblages, and a 400 ka cycle is typically associated with more significant faunal change (Waters and Condon 2012). The combined influence of sea level fluctuation with proximity to delta systems generated lateral and stratigraphic heterogeneity in the preserved organic fraction (Gross et al 2015; Emmings et al 2020b).

Emmings et al (2020a) determined that the chemistry of the Pendleian water column in the Craven Basin had an oscillating palaeoredox zone which maintained euxinic conditions during transgressive-high stand sea level states, becoming more oxidised with falling or low sea level states. Similarly Arnsbergian mudstones from the distal Widmerpool Gulf were deposited under anoxic conditions which extended to the photic zone during high sea levels, with low sea level associated turbidite sediments associated with increased volumes of terrestrial organic matter, reduced salinity and more dysoxic to oxic conditions prevailing in the water column (Gross et al 2015).

Oxic or aerobic water is classified as containing over 2 mL/L of oxygen, representing well-ventilated water inducing no biological stress on fauna and enabling degradation of dispersed organic matter in sediment (Algeo and Li 2020). Anoxia represents the total lack of dissolved oxygen, conditions which

are often associated with the biological use of sulphate in oxidation-reduction reactions (Algeo and Li 2020). Anoxic conditions are ferruginous if dissolved Fe^{2+} is present, or euxinic if H_2S is present instead (Algeo and Li 2020). Dysoxia is a commonly applied term in geoscience, which relates to the impact of reduced oxygen levels (2-0.5 mL/L) to fauna distribution and diversity and organic enrichment (Tyson and Pearson 1991). Sub-oxic is used to describe water with very low (0.7-0 mL/L) oxygen concentrations, where the depositional environments lacking significant bioturbation and macro-fossils (Tyson and Pearson 1991; Breck 1974) and reduction reactions involving nitrate, manganese or iron are facilitated by microbial organisms.

Biomarkers, represent the biomolecular record of organisms existing within the depositional regime in which sedimentary rocks are deposited. Some biomarkers such as Pr/Ph may be interpreted as indicative of palaeoredox conditions (Didyk et al 1978). Published values for Pr/Ph ratios are shown on Figure 1 where oxic waters are represented by values over 3, dysoxic-sub-oxic as values between 2 and 0.8 while anoxic to euxinic values will be lower than 0.8. Other biomarkers such as Aryl Isoprenoids have been proven to represent the presence of water column euxinia which extends to the photic zone (Schwark and Frimmel 2004; Gross et al 2015). The change of Aryl Isoprenoids has also been included in Figure 1. High levels of C_{35} homohopanes has also been related to the presence of anoxia, as the hopanes are more likely to have been originated from bacterial groups. Ts/Tm as a biomarker index may also demonstrate Eh effects at the sediment water interface if it is anoxic (Peters et al 2005).

In the current study, 201 samples from the Central Pennines and Craven Basin were analysed to develop a spatially distributed dataset on biomarker environmental indices, representing the first study to analyse organic geochemical trends across multiple boreholes dated from the Brigantian to the Arnsbergian-Chokerian boundary. To relate the study to other regional works, programmed pyrolysis was undertaken on all samples to understand the bulk geochemical source rock character of Mississippian mudstones. Biomarker results were produced from extractable organic matter (EOM) to delineate changes pertaining to salinity, water column anoxia, and the provenance of organic matter across the basins.

Geological Setting

The Carboniferous Basins of northern England began rifting in the Devonian, relating to collapse of the Caledonian Orogen following the closure of the Iapetus Suture (Fraser and Gawthorpe, 2003). The Late Devonian-Carboniferous subduction of the Rhenohercynian oceanic crust contributed to additional thermal and magmatic input, generating crustal stretching and Dinantian rift basin formation (Timmerman 2004; Leeder 1988). Far-field orogenic influences contributed transtensional forces enabling periodic eastward extension through which compression is accommodated via 'crustal escape' or extrusion mechanisms, (Maynard 1997; Fraser and Gawthorpe, 2003).

Rifting initiated over continental conditions, with subsidence enabling the formation of lacustrine and transgressive horizons within the Devonian sequences. By the Early Carboniferous, marine to periodically sub-aerial conditions were established depositing the Carboniferous Limestone Supergroup of Waters et al (2009). The earliest stratigraphy was dominated by regional shallow water carbonates. This depositional environment persisted on the shelves while the basins rifted forming ramp and slope architectures into the depocentres (Fraser and Gawthorpe. 2003, Riley, 1990). The margins would periodically collapse into the depocentres forming a framework of calciturbidites and other transport deposits interbedded with calcareous mudstones.

The Bowland Shale formation and its diachronous counterparts were deposited under late synrift and early postrift conditions, onlapping the carbonate margin sediments (Waters et al 2020b). The source rock interval was confined to the basin depocentres during the Dinantian, but 'drowning' of palaeohighs enabled draping of the source rock onto the carbonate highs (Waters et al 2020b; Kirby et al 2000). Palaeowater depths of depocentres were interpreted to be >300 m by Fraser and Gawthorpe (2003).

Siliclastic turbidites acted as precursors to basin infill by the deltaic Millstone Grit Group (Waters et al 2020b). Infill of the basins occurred in a stepwise staged process as carbonate highs provided a barrier directing sedimentation through erosional valley systems (Waters et al 2020b; Fraser and Gawthorpe 2003), generating diachroneity in the age at the top of the Bowland Shale. Within the Millstone Grit Group periods of deltaic influence were broken by the deposition of organic rich mudstones such as the Caton Shales (Clarke et al 2018) extending source rock deposition into at least the late Arnsbergian (Waters et al 2020b). Within the Widmerpool Gulf Arnsbergian age sediments are represented by the Morridge Formation, which includes distal turbidites and hemipelagic mudstones (Waters et al 2009). Brigantian to Pendleian mudstones from the Craven Basin contain a relatively high detrital mineral fraction and an associated mixed type II/III organic matter composition, particularly in the Upper Bowland Shale (Clarke, et al 2018). Palynological interpretation of their Widmerpool Gulf counterparts revealed a plethora of microbially degraded organic matter types, and evidence of algal groups such as *Botryococcus* spp. (Konitzer et al 2016; Hennissen et al 2017; Hennissen et al 2020).

Experimental

Core logging, sampling and preparation

Boreholes held at the National Geological Repository core store in Keyworth were studied during the project. Cores were selected based on whether they contained representative samples of Carboniferous mudstones. The cores were required to have been tied to the goniatite biostratigraphy of the UK Carboniferous, through either core logs available via the BGS GeoIndex, industry reports available through the UK Onshore Geophysical Library (UKOGL), academic papers or PhD theses. Core chips were taken where possible at regular intervals through the cores.

Core chips were washed with *n*-pentane to remove any surface labile hydrocarbons and contaminants. The samples were powdered using a ceramic mortar and pestle, to an approximatte <30 μm size. A single powdered aliquot for the current study was produced, weighing approximatel y 3-5 g. This was split as required for Rock-Eval(6), and solvent extraction ahead of biomarker analysis.

Rock-Eval(6) Programmed Pyrolysis

Programmed pyrolysis is a commercially available standard methodology for studying source rock quality and richness through the measurement of produced volatile products such as hydrocarbons, CO_2 and CO, from the staged heating of sample material (Espitalié et al 1977; Lafargue et al 1998). The measurements of pyrolytically released volatiles are often compared to determine the kerogen types and whether the rock is prone to producing gas or oil (Peters et al 2015; Jarvie 2012). Furthermore, the temperature at which maximum hydrocarbon generation occurs (Tmax) is known to relate to the maturity of samples as an alternative to vitrinite reflectance (Espitalié 1986). The use of the method formed a central focus of many Bowland Shale specific studies (i.e Newport el al 2020; Hennissen et al 2017; Gross et al 2015; Waters et al 2020b), thus the analysis from this project provides a direct comparison to other regional studies. This project made use of the Rock-Eval(6)

pyrolysis and oxidation capabilities hosted at the British Geological Survey, to standardise and compare measurements with published results such as Waters, et al (2020b).

Powdered aliquots of samples were analysed using a Rock-Eval(6) analyser configured in standard mode, pyrolysis and oxidation as a serial process (as in Waters et al 2020b). Powdered rock samples were heated isothermally and maintained for 3 minutes at 300 °C to release free hydrocarbons. Subsequently a heating ramp of 25 °C/minute was used to increase the temperature from 300 to 650 °C cracking non-volatile organic matter in an inert atmosphere of N_2. Hydrocarbons released from this process were measured using a flame ionising detector (FID), and CO with CO_2 were measured using an IR cell. From the pyrogram FID and IR peaks, the S1, S2 and S3 parameters were given and used to calculate hydrogen index (HI), oxygen index (OI), and production index (PI) as per the equations in Lafargue et al (1998). After pyrolysis the samples are oxidised from 300 to 850 °C to determine the residual carbon in the rock, which was used with data from the S2 and S3 peaks to derive the TOC content.

Gas Chromatography-Mass Spectrometry (GC-MS)

Around 1 to 1.5 g of powdered aliquot were added to clean test tubes, with 10 μL of a prepared internal standard of squalane and *p*-terphenyl. 4 ml of dichloromethane (DCM)/methanol 93:7 v:v were added to the samples, which were subjected to 5 minutes of sonication and centrifuged for 3 minutes at 1.5 rpm. The resultant supernatant was transferred into a new test tube and the process repeated 4 times per sample. Copper turnings were added to the supernatant and the volume was reduced and replaced with DCM:*n*-hexane 1:1 v:v mixture before the aliphatic and aromatic fractions were eluted using DCM:*n*-hexane 1:1 v:v by column chromatography using activated alumina powder. The fraction was further concentrated to 0.5 ml.

Analysis was conducted using an Agilent Technologies 7890A GC system coupled to a 5975C mass spectrometer. The GC injector was run in a splitless mode (1 μL) with the column flow rate set at 1.1 mL/min. A J&W scientific DB-5MS capillary column was used for compound separation and helium employed as a carrier gas. GC oven was started at 40 °C for 2 minutes, this was raised at a rate of 5 °C/min[-1] to 310 °C and held for 14 minutes. Mass spectra were acquired in electron impact mode in the scan range of 50-500 amu. The data was qualitatively and quantitatively studied using the Mass Hunter workstation software package. Biomarkers were identified and indices were determined by comparative investigation of peak areas for each chromatograph produced.

X-Ray Diffraction

X-Ray Diffraction (XRD) analysis was completed using a PANalytical X'Pert Pro Alpha-1 system hosted at the Natural History Museum, London. The unit was set up with a cobalt source tube which recorded a diffraction angle range from 4° to 90°. For each analysis 1 g of powdered sample material was backloaded into metal holders. Mineral peaks were picked using the XPERT Highscore Plus software package, and samples were quantified utilising PROFEX open source XRD rietveld refinement software.

Samples and stratigraphic correlation

The 201 samples included in the current study were taken between 9 boreholes in northern England, either at equivalent ages or a range of depths to determine variation in biomarker trends temporally and spatially. The distribution of cores versus time is illustrated in Figures 2 and 3. From core material dated to the Arnsbergian or younger, 141 samples were taken, mostly focussing on the

Carsington Dam Reconstruction-C4 (n=53) and the Wray boreholes (n=47). The Pendleian to Brigantian had a total of 60 samples taken between 4 boreholes. The distributions of samples is shown in Figures 2A and 3A showing well locations, and Figures 2B and 3C demonstrating sampling locations against sedimentary logs.

In the Wray geothermal borehole, the E_{2b} marine band is marked by the identification of *Cravenoceras subplicatum* at ~120.45 m (Brandon et al 1998). Beneath the E_{2b} marine band, the Wards Sandstone representing a delta top would have eroded any coeval representation of the E_{2a3} *Eumorphoceras yatasae* marine band. The underlying siltstone facies represent the Close Hill Siltstone and may contain the E_{2a2b} marine band of Brandon et al (1995). This borehole represents Arsnbergian strata in the Craven Basin allowing correlation with datasets from the Widmerpool Gulf equivalents.

The Croft House borehole sited upon the Askrigg Block encountered similar strata to the Wray Geothermal borehole. The E_{2b} marine band is attributed to 40-42 m depth as in Brandon et al (1995). This is positioned above the Red Scar Grit, and E_{2a} equivalent shales which relate to the Wards Sandstone and Close Hill Siltstones of the Wray Geothermal borehole.

In the Carsington Dam Reconstruction-C4 borehole the E_{2b} marine band is recognised through the presence of *Cravenoceratoides edalensis* from 22.52 m, with Cravenoceratid fragments first appearing from 26.67 m. The E_{2a3} marine band is present in this borehole and was logged by Konitzer et al (2014) from ~27.9 to 33.85 m. Both E_{2a2a} and E_{2a2b} marine bands were first correlated between the Carsington Dam locality, the Duffield borehole and the Bowland basin by Brandon et al (1995), Konitzer et al (2014) logged an unidentified E_{2a2} marine band from 52.6 to 53.1 m in the borehole. Based on published logs this is likely to be the E_{2a2b} marine band (Brandon et al 2015). At the Carsington locality, the borehole records no delta top sandstone and represents a distal setting with consistent marine conditions influenced by siliclastic turbidites (Konitzer et al 2014). Rempstone-1 was also logged and studied which represents E_2 mudstones in a turbiditic setting.

The logged section of the Ipstones Edge borehole contains the *I. subglobosum* H_{1a1}, and the E_{2c2-4} Nuculoceras nuculum marine bands (Chisholm et al 1988; Morton et al 2015). The lower section of the borehole is divided by the Hurdlow Sandstones, which are described as a turbiditic unit found in the Goyt Trough and western Widmerpool Gulf (Morton et al 2015). The Hurdlow Sandstones overly an undated mudstone, which is tentatively assigned to the E_{2b3} zone.

Waters et al (2020b) highlighted that in the Widmerpool Gulf, only samples below the E_{1b2} *Tumulites pseudobilinguis* marine band can be considered as being representative of the Bowland Shale Formation and that strata younger than that horizon should be considered as representative of the Morridge Formation. To test similarities of conditions within the Widmerpool Gulf the Lees Farm borehole was studied. From borehole reports the Lees Farm borehole has the E_{1a} marine band sited at 12.7 m depth, recognised by *Emstites leion* at 11.18 m depth. Below which at 23.30 m depth *Neoglyphioceras* Sp. represents P_2 zone Brigantian age strata diachronous with the Lower Bowland Shale. The Wardlow Mires boreholes were sited on the Derbyshire High recording strata from the E_{2a} *Eumorphoceras bisculatum* zone to the P_2 zones represented by *Neoglyphioceras* Sp. and *Sudeticeras* Sp.

The Marl Hill 4 borehole has been extensively studied and the biostratigraphic positioning is based from the resulting publications (see, Emmings et al 2019; 2020a; 2020b). This puts the E. Leion E_{1a} zone at ~17 m depth marking the boundary of the Upper and Lower Bowland Shale as they appear in

the Craven Basin. Cominco-S3 provides an equivalent representation of this boundary at 13.72 m depth for comparison. At 31.50 m depth in the Cominco-S3 borehole the P_{2b} to P_{2c} boundary was interpreted based on the upper observation of *Neoglyphioceras* Sp. representing the Mid-Brigantian.

Results

TOC Content and Programmed Pyrolysis

The whole dataset of samples has a mean average TOC content of 3.14 %, which ranges from 0.42 % in the Croft House borehole to 20.16 % in the Wardlow Mires core. Splitting the sample set into regions, gives an average TOC content of 3.08 % in the Craven Basin and 3.20 % in the Central Pennines. In terms of the cores sampled in the Craven Basin, Cominco-S3 had the lowest average at 2.63% and Croft House had the highest average TOC at 4.37 % . Comparatively in the East Midlands, Ipstones Edge had the lowest of sampled wells at 1.80 % while Rempstone-1 had the highest mean TOC content of 5.74 %. Figures 2 and 3 show TOC contents for the different boreholes, comparatively the values show an overall greater abundance of TOC in the Widmerpool Gulf in comparison to the Craven Basin.

The S2 results from the total data give an average value of 5.52 mg HC/g rock. In ™ Craven Basin the average value decreases to 2.92 mg HC/g rock, ranging from 1.70 mg HC/g rock in the Wray borehole to a high average of 5.61 mg HC/g rock in Marl Hill-MHD4. In the Central Pennines, the mean S2 is 7.60 mg HC/g rock, ranging from 1.86 mg HC/g in the Ipstones Edge borehole to 25.53 mg HC/g rock in Rempstone-1.

Tmax results vary across the sample set between 421 °C in the Ipstones Edge borehole, to 464 °C in the Cominco-S3 borehole. The mean value across all samples is 438°C. Tmax was found to vary significantly within boreholes, for example the Wardlow Mires core has a minimum Tmax of 427 °C at 8.71 m MD to 452 °C at 105 m MD (Figure 3B). Such a variation in Tmax results is assumed to be incorrect for a standard geothermal gradient, which is attributed to lower S2 values associated with turbiditic and deltaic samples as in Figure 2B, 2C, 3B and 3C.

An average HI value of 144 mg HC/g TOC was calculated for the dataset (Figures 2c and 3c), split between a mean of 196 mg HC/g TOC in the East Midlands Samples and 88 mg HC/g TOC in Lancashire-Yorkshire. The Wray borehole had the lowest HI at 66 mg HC/g TOC (Figure 2B), while Rempstone-1 had the highest mean at 403 mg HC/g TOC (Figure 3B). Plotting HI against Tmax (Figures 2C and 3C) to determine maturity and kerogen type demonstrates a distribution of data points in the immature to mid-oil window, varying between Type II and III kerogen classifications. From the S3 data, OI was calculated for all samples with a mean value of 19. Within the dataset 10 samples have OI values over 40 mg CO_2/g TOC.

Acyclic isoprenoids and *n*-Alkanes

Both pristane and phytane were detected in all samples, the ratio of these ranged from 0.62 to 6.92 with a mean value around 1.55, which correlates with values previously published from the Craven Basin (Emmings et al 2020a). Most samples were distributed within values of 0.8-1.8 (Figure 3B, 4B). Comparing the isoprenoids in Figures 4A and 5A to their *n*-alkane counterparts *n*-C_{17} and *n*-C_{18}, most samples have a ratio of less than 1. Samples mostly from the boreholes Croft House and Ipstones Edge plot above 1, alongside many of the Lees Farm borehole samples. The majority of samples fall into a mixed organic matter type, and a mixed oxidising-reduced setting according to those ratios.

The aliphatic content of the samples EOM contained a suite of n-alkanes from n-C_{11-35}, although the higher abundances generally ranged from n-C_{13} to n-C_{33}. The percentile distribution of n-alkanes is orientated toward C_{11-20}, with C_{21-25} representing the second highest distribution. This is reflected in calculated carbon distributions such as the Terrigenous to Aquatic Ratio (TAR) in which most data points range below a ratio of 1 (Figure 4B and 5B). Carbon Preference Index (CPI) results range within boreholes as shown in Figure 4B but modally plotted close to a value of 1 for the Brigantian-Pendleian samples and were slightly elevated for Arnsbergian sample material (Figure 5B) indicating a slight odd preference consistent with additional terrigenous organic matter.

<u>Hopanes, Terpanes and other 191 mass chromatogram peaks</u>

The 191 terpane chromatogram is dominated by hopanes. Tricyclic and tetracyclic terpanes are also present, as shown in Figure 6 but were not quantified. 17α-trisnorhopa™Tm) and 17α-trisnorneohopane (Ts) were detected in all samples with a slight preference to Tm in the peak heights. On average the C_{30} 17α-21β-hopane homologue has preference over C_{29}αβ. While the C_{31-35} homohopane series has a stepwise downward trend through the homologues from C_{31} to C_{35}. This produced an average C_{35} homohopane index of 7% rising to a maximum of 16% in the Carsington Dam Reconstruction-C4 borehole, and minimum of 4% in the Wray borehole. Comparing hopane homologue ratios shows a mean $C_{31}R/C_{30}$ of 0.30, a mean C_{35}/C_{34} of ratio of 0.31 and for C_{29}/C_{30}: 0.77. Hopane isomerism shows a preference in the chromatograms toward the S isomer, this is reflected in the 22S/(22S+22R) indices which average 0.59 for C_{31}, 0.57 for C_{32} and 0.54 for C_{33}. C_{35} hopane isomerism averages significantly lower than the other indices due to low concentrations and thus is not interpreted further. C_{34} isomerism is higher, averaging 0.64 for the whole sample set.

Rearranged hopanes were also observed in trace quantities. The C_{29} 18α(H)-30-norneohopane (C_{29}Ts) coeluted with C_{29} 17α-21β-hopane and was quantified by the area of the peak shoulder effect produced. The C_{30} 18α(H)-30-neohopane (C_{30}Ts) was identified by its relative retention indices to the C_{29}Ts shoulder and C_{30}ab hopane. C_{30} and C_{29} 17α-diahopanes were widely observed. Trace doublet peaks between the C_{32}-C_{35} homohopane doublets (Figure 6) may represent the presence of a diahopane homologue series. Additionally a small peak representing a trace amount of C_{28} 28-norhopane was commonly observed eluting between C_{29} diahopane and C_{29}αb/Ts, it was confirmed through a m/z 355 EIC.

In addition to the hopane series, gammacerane was also widely detected with a relatively small peak area (Figure 6) in the samples analysed. The gammacerane index (GI) was calculated as 10xgammacerane/(gammacerane+C_{30} hopane). The average value for the sample set is ~1. The range of values includes a maximum of 2.68 and minimum of 0.34, both values were recorded from the Carsington Dam Reconstruction-C4 borehole, but most samples across the entire set distribute between 0.5 and 1.5 GI. GI varies stratigraphically, enhanced levels occur around marine bands found in Cominco S3, Marl Hill 4, Ipstones Edge and Carsington Dam Reconstruction-C4.

<u>Steranes</u>

The most common steranes in the EOM analysed were the C_{27}-C_{29} sterane homologues (Figure 7). Of the steranes quantified there was a preference in the samples toward C_{29} which contributes a mean 43% of the total C_{27-29} sterane homologue content. The C_{28} sterane accounts for the lowest percentile of the steranes analysed. C_{27} has a mean of ~35% of the total sterane homologue content. In the ternary plots in Figure 4A and 5A the samples show a central distribution between C_{27} and C_{29} which fits into a mixed *Planktonic/Bacterial/Land Plant* organic matter zone.

Comparison of the m/z 217 and 259 EIC's in Figure 7 demonstrated that a number of peaks represent diasteranes, or a coeluted mix of steranes and diasteranes. Affected sterane peaks observed include but are not limited to: $27\alpha bbR$, $27\alpha\alpha\alpha S$ and $28\alpha bbR$. The coelution of compounds reduced the accuracy of quantification, distorting indices reported from those peak areas. For the purposes of testing the impact of clay mineralogy on organic matter alteration, the ratio of $27b\alpha$ (S+R) diasterane to $27\alpha\alpha\alpha R$ sterane was used in place of conventional ratios. This was due to the fact these peaks have been influenced the least by coelution. For comparison of sterane abundances the $\alpha\alpha\alpha R$ sterane peak was used.

Some lower mass peaks visible in the m/z 217 EIC were tentatively assigned to the C_{22-33} sterane/diasterane homologues, but were not interpreted in the current study. After the C_{29} $\alpha\alpha\alpha 20R$ sterane there are a number of peaks indicative of C_{30} steranes (Figure 7). Interpretation of the C_{30} sterane peaks was tentative as the peaks coeluted with other compounds, thus they were not quantified for the current study.

<u>Aryl Isoprenoids and other observed aromatics</u>

Peaks representing a suite of aryl isoprenoid compounds with carbon numbers from C_{11} to C_{27} were recognised through comparison of the m/z 133 and 134 EIC's as in Figure 8. Peak areas for some of these compounds were quantified to produce the Aryl Isoprenoid Ratio (AIR) after Schwark and Frimmel (2004), calculated as $(C_{13-17})/(C_{18-22})$. Of the 200 samples analysed through GC-MS methods, only 123 samples had aryl isoprenoid peaks. None of the samples from the Warlow Mires-1 and Cominco-S3 boreholes had quantifiable peaks, and only 4 samples from the Croft House core and 12 from Wray were quantifiable. The AIR across all measured samples ranges from 0.16 in the Ipstones Edge Borehole to a maximum of 16.78 in the Carsington Dam Reconstruction-C4 borehole. Marl Hill and Lees Farm boreholes made up the lower range values, while Carsington Dam Reconstruction-C4 and Rempstone-1 contributed the most to the higher range. The precursor molecule for the aryl isoprenoids was not confirmed through isotope ratios, thus a β-carotane precursor cannot be ruled out. Neither β-carotane or Isoreniaretane were identified in any samples, and likely remains within the kerogen structure due to the low maturity of material sampled.

As can be seen on Figure 8 the m/z 133 EIC shows a range of additional peaks alongside the aryl isoprenoids. Mass chromatograms were checked against other aromatic compounds, finding matches through the m/z 204 and 205 EIC showing coelution of C_{15} isohexyl alkylaromatics. Additionally, through the m/z 246 EIC phenylalkanes were observed, in particular C_{18} phenylalkane.

<u>Mineralogy from XRD</u>

X-Ray Diffraction analysis as summarised in Figure 9, showed a primarily clay to silicate rich composition. Two samples from Carsington Dam Reconstruction C4 plotted as being carbonate rich. The distribution of datapoints matches those published by Hennissen, et al (2017). Two mineralogical populations were determined, Arnsbergian samples from Rempstone-1, Wray, and Carsington Dam Reconstruction-C4 were found to commonly contain a clay rich and carbonate poor mineralogy. The second population is made of samples from Carsington Dam Reconstruction-C4, Lees Farm-1 and Marl Hill MHD4, this plots under a siliceous mudstone category and matches average data for the Barnett.

Clay mineral type is comprised of a mixture of expandable clays, classified through Profex as smectites combined with illite. Attempts to distinguish maturity levels were not possible due to mixed layering of the expandable clay fraction. Kaolinite was commonly observed in the samples, but

quantification was complicated as the peaks were shared with chlorite which was mostly present in Arnsbergian aged samples.

Carbonate mineralogy changes across the sample set dependent on location. Carsington Dam Reconstruction C4 contained a mix of calcite and ankerite, which was also observed by Hennissen, et al (2017). Lees Farm was found to contain peaks correlating to dolomite. Marl Hill Moor MHD4 contained only calcite. The Wray borehole only had calcite in two samples which correlated to the marine band in the top of the cored section. Trace to 5 % concentrations of siderite was observed in samples from Rempstone-1 and in turbidite facies belonging to the Wray borehole.

Pyrite was commonly measured in the samples. The highest pyrite contents were recorded in Marl Hill Moor MHD4, which had a range from 1 to 11.64 %. Pyrite was commonly associated with samples originating from marine facies. Very little pyrite was recorded in the Wray borehole, consistent with its common terrestrial kerogen classification. Anatase was also commonly observed in most samples but in low to trace abundances (<5 %).

Discussion

Overall source rock potential from bulk geochemistry

The average TOC contents for the sampled cores may be defined as 'good' to 'very good' (Peters 1986), with the average values above the proposed cut-off of 2% by Andrews (2013). According to the S2/TOC biplots in Figures 2C and 3C only 40 samples fell below the 2 % cut-off. However, the volume of TOC that can generate hydrocarbons has a greater significance to source rock potential than the presence of any TOC.

Correlation of TOC content and S2 (Figure 2C and 3C), shows that the samples from each basin distribute slightly differently. The Bowland basin samples have a significantly lower S2 to TOC correlation than the samples from the East Midlands. Overall the majority of datapoints align with published data with samples analysed in this study matching argillaceous/terrestrial organo-facies (Emmings et al 2020a; Newport et al 2017). The Arnsbergian aged samples (Figure 3C) closely matched trends from the Duffield, Carsington Dam Reconstruction-C3 and C4 boreholes.

Interpreting organic matter source from the S2-TOC plots in Figures 2C and 3C, suggested that the samples were mostly comprised of either 'mixed' type kerogens or type III and IV. These kerogen types would not fit with the required standards for a shale play in the UK (Andrews 2013). HI-OI plots show that many of the samples plot close to the axis intercept for both sample sets, indicating a low generative potential (Figures 2A and 11his This demonstrated some relationship to facies whereby samples from turbidite and hemipelagite facies had the lowest potential. Marine Band facies were always found to have the highest HI to OI ratio. Data points typically follow the maturation trend lines for either Type II or Type III source rocks. Only a few samples exceed HI values of 300 mg HC/g TOC, which would make for a suitable shale gas target (Andrews 2013).

The poor generative potential represented by HI or S2 values demonstrated that the TOC content present had a low pyrolytic potential. Palynological analysis of the Carsington Dam Reconstruction-C4 borehole (Konitzer et al 2016) interpreted that dispersed organic matter was distributed by suspension settling of granular amorphous material. The organic matter has been reported to represent biotic degraded organic matter with observation of aliphatic rich material supported in faecal matter (Emmings et al 2019). Newport et al (2020) interpreted the Bowland Shale Formation of the Marl Hill 11 borehole to have a high oil yield from primary generation based on relative proportions of type I

and II kerogens. Modelling and pyrolysis experiments on kerogen extracts from the Widmerpool Gulf showed high primary generation and expulsion, however secondary gas generation was regarded as a significant contribution to the hydrocarbon yield (Yang et al 2016). Hennissen et al (2020) observed fluorescence and Type I macerals such as *Botryococcus* sp. in Arnsbergian aged rocks, which would support the argument that Carboniferous shales have a high primary oil producing capability. The above studies did not report significant quantities of inertinite matter, which could be regarded as candidate for enhanced TOC contents in low S2 yield samples.

General environment of deposition

Extracting information about the environment of deposition from programmed pyrolysis data is tentative, presenting difficulties with estimating kerogen type and generative potential. Studying the molecular representation of organisms, biomarkers, is a means to determine the environmental conditions under which a source rock was deposited.

Using Pr/Ph as a palaeoredox index (Didyk et al 1978), the mean average of the sample set (1.55) falls within the 'dysoxic' window. Comparison of these acyclic isoprenoids and their *n*-alkane counterparts (Figures 4A and 5A) support the dysoxic interpretation. The mean of the dataset is similar to averages from the Marl Hill-4 borehole (Emmings et al 2020a), the Duffield borehole (Gross et al 2015) and Malton-4 (Slowakiewicz et al 2015) highlighting that reducing conditions were prevalent across the Carboniferous seaways present in northern England. Predominance of C_{31} over C_{35} hopane homologues seen from chromatographs can indicate sub-oxic to oxic conditions, although the ratio is impacted by thermal maturity and mineralogy (Peters and Moldowan 1991).

Identification of trace amounts of aryl isoprenoids supports the evidence that reducing conditions were present and contributed to the water column chemistry (Figure 10). Reducing conditions detected via low Pr/Ph supported more stable photic zone euxinia evidenced by a prevalence of long chain aryl isoprenoids in Figure 10 (Schwark and Frimmel 2004). Evidence of combined dysoxia and euxinia refers to zonation in the water column. During deposition, a thicker euxinic water column would have been present representing poor ventilation of bottom waters. Organic matter produced by surface productivity was decomposed by sulphate reducing bacteria at the sediment-water interface, recognised from samples at Marl Hill 4 (Emmings et al 2020a). Samples representing more oxidising environments in Figure 10 showed a predominance of shorter chain aryl isoprenoids indicating that at locations where they could be detected, photic zone anoxia was likely to be episodic and organic matter was exposed to oxidative degradation for extended periods of time (Schwark and Frimmel 2004). Group 1 represents marine facies i.e. marine bands, hemipelagite and carbonate slope, all associated with indicators of persistent euxinia extending to the photic zone. Turbidite facies form Group 2 on Figure 10, representing episodic photic zone anoxia consistent with ventilation of the water column during low stand sea levels (Emmings et al 2020a; Gross et al 2015). Ventilation of the water column enabled degradation of the aryl isoprenoid chains (Schwark and Frimmel 2004) likely during the same periods that contributed to microbial sediment water interface effects as in Emmings et al (2020b).

Gammacerane supports the interpretation of a stratified water column (Sinninghe Damste et al 1995), however the values do not vary significantly through the dataset and no major peaks were detected from the 191 EIC's. Gammacerane is commonly associated with bacteriovorous ciliates living beneath chemoclines (Harvey and McManus 1991; Sinninghe Damste et al 1995) often connected with, but not limited to hypersaline environments (Peters et al 2005). The concentrations reported in the current study do not provide evidence for hypersaline conditions. Other influences must have

generated stratification i.e. thermal layering (Emmings et al 2020a). GI versus Pr/Ph in Figure 4A shows that there is a slight relationship between Pendleian-Brigantian reducing conditions and water column salinity. Most samples as in Figure 5A suggest dysoxic saline conditions prevailed during the Arnsbergian.

From 51.6 m in the Carsington Dam Reconstruction-C4 log there is a significant excursion of GI values. is following from the proposed location of the E_{2a2b} marine band at 52.6-53.1 m (Konitzer et al 2014; Brandon et al 1995). Gross et al (2015) provides no data or interpretation on that minor cycle. The excursion coincides with the onset of low sea level conditions and deposition of distal turbidites potentially connected to the uppermost Duffield Turbidite (Aitkenhead 1977). Konitzer et al (2014) described bioturbated and lenticular facies indicating enhanced sediment-water interface oxygenation, proven here by relatively higher Pr/Ph. The excursion is interpreted as being representative of sea level fall, and development of a substantial oxygenated freshwater lense across saline bottom waters in the Widmerpool Gulf. This is the only significant salinity stratification observed from the gammacerane data in the current study. Aryl isoprenoids were detected in this layer, with a relatively high AIR, ranging from 3.05 to 8.33, plotting in Group 2 on Figure 10. Any anoxia present would have been highly episodic with a ventilated water column, anoxia would have been driven by productivity in the surface water layer (Emmings et al 2020b).

Origin of organic matter

Most samples have a Pr/n-C_{17} and Ph/n-C_{18} ratio <1 which in this case was interpreted as being representative of an algal or microbial short chain alkane origin, as was suggested for the Duffield borehole by Gross et al (2015). Such a trend could be generated by maturity, but would not be expected within early oil window samples. Analysis of the distribution of the n-alkanes further supports the aquatic organic constituent source. The TARs reported in Figures 4B and 5B are <1 indicating an aquatic origin. Meanwhile the CPI is approximately 1 for many samples, indicative of marine conditions and no preference in chain length. Locations such as Wray, Croft House and Rempstone have slightly higher CPI value distributions (>1), which would be consistent with terrestrial organic contribution represented by the deltaic derived detrital sandstones logged from the core material available. The tentative observation of C_{30} sterane peak areas in the samples is further evidence for a marine organic source (Moldowan et al 1985; Peters et al 1986).

Predominance of the C_{29} sterane isomers over other sterane groups in the samples was interpreted to be representative of terrestrial organic matter (Volkman 1986). However the samples relate to a planktonic/bacterial/land plant window suggestive of organic mixing. Some of the potential aromatic molecule candidates present alongside the aryl isoprenoids on the m/z 133 EIC, could be representative of isohexyl alkylbenzenes such as $C_{15}H_{24}$ 1,3,4-trimethyl-2-(4-methylpentyl) benzene. Isohexyl alkylbenzenes are indicative of higher plant or microbial input (Ellis et al 1996; Wang et al 1990), both of which are viable explanations based on the organic macerals representing bacterial degradation of terrestrial matter described by Konitzer et al (2016).

In agreement with observations from Gross et al (2015) the general organic source was mixed. Algal and bacterial markers such as short chain alkanes, tricyclic terpanes, and C_{27} steranes provide a strong indicator of organic matter akin to type II kerogens. This interpretation is consistent with palynological observation (Konitzer et al 2016; Hennissen et al 2017; Newport et al 2020) and interpretation of the source rocks activation energies (Yang et al 2016; Newport et al 2020). C_{29} steranes present evidence of terrestrial organic matter which was biotically decomposed as it settled through a stratified water column. Samples from the Widmerpool Gulf show greater variation in the

ratio of C_{27} to C_{29} than their counterparts in the Craven Basin (Figures 4a and 5a). Extracted steranes from the Craven Basin express a slight preference towards C_{29}, which is likely generated by proximity to the Pennine Delta front and resultant consistency of terrestrial organic matter influx and preservation.

<u>Maturity indices and influencing factors</u>

Based on the average Tmax trends for the boreholes in Figures 2B and 3B the samples analysed in this study are early oil to peak oil mature. This is supported by low vitrinite reflectance values for locations such as 0.55 %Ro at Rempstone-1 (Hennissen and Gent 2019; Coombes et al 1986); a calculated %Ro of 0.5-0.8 Carsington Dam locality (Henry et al 2018) and similarly the Marl Hill locality's calculated %Ro of 0.8 (Herrman et al 2018). Some boreholes exhibited anomalous Tmax ranges that were inconsistent with the geothermal gradient and burial depth range of the sampled interval. 14or example Cominco-S3 in Figure 2B has a Tmax range of 20 °C in the upper 20-30 m of the cored section. As the samples are within the oil window they are not interpreted directly as a shale gas resource, and should not exhibit such high maturities.

Biomarkers also provide maturity data, through effects such as preferential thermal degradation or isomerism of compounds. Figure 11 shows biomarker maturity indices plotted against Tmax revealing a range of either correlating or contradicting relationships. Firstly, the hopane inventory (Figure 11A) of the samples had reached hopane isomer equilibrium indicating that the source rocks were at an oil expulsion maturity level. Moretane ratios were also determined to have achieved full maturity with no apparent relationship to Tmax. However, Ts/Tm (Figure 11C) shows no Tmax relationship and a low to moderate maturation level.

Influences from the environment of deposition are the most likely cause of these trends. The moretane ratios indicate a predominance of C_{30} hopane over moretane. Rulkotter and Marzi (1988) observed high moretane values in hypersaline rocks, while Isaksen and Bohacs (1995) observed enhanced moretane ratios in highstand as opposed to lowstand tracts which was attributed to higher plant contributions. It would be a reasonable hypothesis to expect such a trend in the Carboniferous mudstones. However, the generation of moretane can also be attributed to bacteria in oxidising sediments as well as diagenetic effects under certain clay types (French et al 2012; Wang, 2007; Quirk et al 1984; Uemura and Ishiwatari 1995).

A predominance of Tm over Ts may relate to either immaturity, oxidising environments or variations in clay influence (McKirdy et al 1983; French et al 2012; Peters et al 2005; Waples and Machihara 1990). Figure 11C shows no relationship between Tmax and Ts/Tm highlighting the low maturity of the samples, and emphasising that alternative influences must have a control on the ratio. Ts/Tm has a complex relationship with Pr/Ph. In the Wray geothermal borehole (Figure 5B) Ts/Tm increases above the E_{2b} marine band indicating enhanced reducing conditions at the sediment water interface. This is likely to be connected to sulphate reduction during flooding of shelf or delta proximal areas as suggested by Emmings et al (2020a). In the Widmerpool Gulf at the Carsington Dam Reconstruction C4 locality samples above the E_{2b} marine band have a reduced Ts/Tm correlating with reduced Pr/Ph consistent with a switch to carbonate pH effects in porewater (Figure 1) (Moldowan et al 1994). The Pendleian-Brigantian samples in Figure 3B show elevated Ts/Tm ratios consistent with widespread Eh effects in porewater during the LMississippian. Carbonate influences are demonstrated in the lower 10 m of Wardlow Mires.

Figure 12A, highlights three populations of samples based on the relationship of Ts/Tm and diasteranes. Group 1 represents anoxic marine conditions whereby organic matter is deposited under euxinic conditions with a moderate flux of detrital clays during marine band and high stand sea levels. Group 2 represents deposition under dysoxic to oxic conditions with samples commonly representing prodelta depositional conditions. Group 3 was defined by the presence of slope, hemipelagite and marine band conditions, representing a setting in which marine organic matter is deposited under euxinia alongside clay input.

The ratio of C_{27} diasteranes to 27 αααR steranes corellates positively to the full range of Tmax values (Figure 12B). As opposed to a maturity relationship the corelation is representative of a mineral matrix effect on programmed pyrolysis results (Espitalie 1986; Peters 1986). The influence interpreted in the current study involved adsorption of free hydrocarbons onto mineral surfaces, decreasing pyrogram peaks and leading to a Tmax shift to high temperatures or poor quality S2 peaks (Espitalie et al 1984; Hu et al 2014; Yang and Horsfield, 2020). Research has suggested that samples with TOC contents over 2 wt.% (Dembicki 1992) and over 0.2 mg HC/g Rock S2 values (Peters 1986) should not be susceptible to the mineral matrix effect. However, data in the current study and palynological data originally observed by Konitzer et al (2016) demonstrated that not all of the TOC is necessarily generative due to biotic decomposition and resultantly the generative fraction can be overwhelmed by the mineral surfaces.

Different facies types relate to diasterane/Tmax trends. Turbidite facies representative of prodeltaic deposition have a strong positive correllation representative of the influence of clay minerals on pyrolysis results. Facies associated with terrestrial organic matter such as deltaic shelf sediments have the highest Tmax results, which was also observed in Emmings, et al (2020a). Marine Bands and hemipelagite facies show a lower influence by clay minerals on Tmax maturity, the trends tend to reverse at boundaries between facies in Figures 3 and 4.

Hopane isomers, in particular the C_{31} and C_{32} homologues typically studied in the samples have reached equillibrium (Figure 11 A and 11C) (Peters et al 2005). The C_{31} isomer ratios in Figure 12C positively correlate with the diasterane ratios used. Fully isomerised hopane homologues in immature sediments have been observed in other basins, i.e. by Moldowan et al (1992) or ten Haven et al (1986). Laboratory experimentation has in the past demonstrated high hopane isomer ratios, that can be 'reset' during laboratory pyrolysis (Peters et al 1990) suggesting high values can be altered by expulsion. Hopane release is in part controled by the breaking of sulphur bonds from kerogen (Koster et al 1997) the nature of which may complicate the ratio. Corelation with diasteranes is indicative of a mineral catalytic effect, or relates to the environment of deposition in a stratified water column that enabled sulphur incorporation into organic mediums. Emmings et al (2020a) reported sulphidic conditions and shallow precipitation of pyrite framboids under high stand sea level conditions, the fully isomerised hopanes in marine band and hemipelagite facies associated with diasteranes may be indicative of sulphur bond influences relating the observations. In the current study pyrite concentrations were noted to be highest in the marine band or hemipelagite facies, further supporting this. In the case of turbidite facies the observed ratio most likely relates to clay catalysis of organic matter. This is supported as turbidite facies plot with the highest clay mineral percentages and diasterane ratios (Figure 12D). Hemipelagite type mudstones plotted with a lower clay to diasterane relationship, while marine bands were more distributed on Figure 12D, reinforcing that Eh to PH effects have a greater influence for those facies.

Studies employing equations to calculate %Ro equivalent from Tmax (using the linear regression modelling) need to consider if the Tmax result is likely to be increased by the mineral matrix effect

giving innacurate maturity trends. Studies such as Andrews (2013) specifically incorporated conversions to establish burial curves for the Upper and Lower Bowland Shale. To counter mineral matrix effects Yang et al (2016) recommends use of kerogen isolates, but the potential of a diagenetic mineral matrix effect on oil window organic matter means that the compositional kinetic pathways of yields from kerogens isolates may be innacurate and not reflective of the true timing of generation vs expulsion.

Maturity results for the Bowland Shale and its diachronous counterparts have been largely misinterpreted in the literature, and care should be taken when using these to aid petrophysical calculations as in Hennissen and Gent (2019). Due to the advanced ratios of certain biomarkers, the samples described in the current study are in the early to mid oil window with an equivelent vitrinite maturity 0.7 to 0.8 % Ro (Peters et al 2005). Low Tmax results in marine band facies were generated by mineral retention effects, and high values in low sea level facies were influenced by the refractory oxidised organic macerals preserved.

Conclusions

The water column conditions as represented by EOM, within the Mississippian basins of northern England are characterised by a continuous dysoxic layer between the sediment-water interface extending euxinia into the photic zone. Influx of terrigenous organic matter and settling of marine organic matter into the basin is proposed to have acted as a feedstock for a bacterial foodweb, leading to the preservation of compounds related to these groups i.e. terpanes, hopanes and gammacerane. The high nutrient load into the basins encouraged the establishment of reducing conditions and switching to sulphate reduction. The kerogen type interpreted from the EOM is a mixed type, but hydrocarbon generative potential at marine band and high stand sea level periods would be akin to type II kerogens despite the mixing.

A mineral matrix effect influences both naturally and pyrolytically matured samples from the current study. Authors using programmed pyrolysis to interpret source rock hydrocarbon prospectivity, or to calculate the orginal parameters should be aware that key values deriving S1 and S2 peaks will be reduced. Further work on hydrous, anhydrous and programmed pyrolysis exploring the role of pyrolysable versus residual carbon in hydrocarbon generation will be required to deduce the importance of this effect for this particular formation. The results of such studies have application to the wider exploration of deltaic derived source rocks where detrital minerals and organic matter are deposited and matured together.

Acknowledgments

References

Aitkenhead, N., 1977. The Institute of Geological Sciences borehole at Duffield, Derbyshire. Geological Survey of Great Britain, Bulletin, 59, pp.1-38.

Algeo, T.J. and Li, C., 2020. Redox classification and calibration of redox thresholds in sedimentary systems. Geochimica et Cosmochimica Acta, 287, pp.8-26.

Andrews, I.J., 2013. The Carboniferous Bowland Shale gas study: geology and resource estimation.

Brandon, A., Aitkenhead, N., Crofts, R.G., Ellison, R.A., Evans, D.J. and Riley, N.J., 1998. Geology of the country around Lancaster. Memoir of the British geological survey, sheet, 59.

Brandon, A., Riley, N.J., Wilson, A.A. and Ellison, R.A., 1995. Three new early Namurian (E1c-E2a) marine bands in central and northern England, UK, and their bearing on correlations with the Askrigg Block. Proceedings of the Yorkshire Geological Society, 50(4), pp.333-355.

Bray, E.E., and Evans, E.D., 1961. Distribution of *n*- paraffins as a clue to recognition of source beds. Geochemica et Cosmicha Acta, 22(1) pp.2-9

Breck, W.G., 1974. Redox levels in the sea. In: Goldberg, E. D. Ed. The Sea: Ideas and Observations on Progress in the Study of the Seas, 5, Marine Chemistry. Wiley, New York, pp.153-179.

Chisholm, J. I., Charsley, T. J., Aitkenhead, N., 1988. Geology of the country around Ashbourne and Cheadle. Memoir of the British Geological Survey, Sheet 124 (England and Wales).

Clarke, H., Turner, P., Bustin, R.M., Riley, N. and Besly, B., 2018. Shale gas resources of the Bowland Basin, NW England: a holistic study. Petroleum Geoscience, 24(3), pp.287-322.

Coombes, D., Hughes, J., Maile, C. N., Batten D. J., 1986. A Geochemical Evaluation of Sediment and Oil Samples from the Well Rempstone-1, East Midlands, UK Land. BP Research Centre, Sunbury-on-Thames.

Dembicki Jr, H., 1992. The effects of the mineral matrix on the determination of kinetic parameters using modified Rock Eval pyrolysis. Organic Geochemistry, 18(4), pp.531-539.

Didyk, B.M., Simoneit, B.R.T., Brassell, S.T. and Eglinton, G., 1978. Organic geochemical indicators of palaeoenvironmental conditions of sedimentation. Nature, 272(5650), pp.216-222.

Ellis, L., Singh, R.K., Alexander, R. and Kagi, R.I., 1996. Formation of isohexyl alkylaromatic hydrocarbons from aromatization-rearrangement of terpenoids in the sedimentary environment: A new class of biomarker. Geochimica et Cosmochimica Acta, 60(23), pp.4747-4763.

Emmings, J.F., Poulton, S.W, Vane, C.H., Davies, S.J., Jenkin, G.,R.,T, Stephenson, M.H., Leng, M.J., Lamb, A.L., Moss-Hayes, V., 2020a. A Mississippian black shale record of redox oscillation in the Craven Basin, UK. Palaeogeography, Palaeoclimatology, Palaeoecology. 538

Emmings, J.F., Davies, S.J., Vane, C.H., Moss-Hayes, V., and Stephenson, M.H., 2020b. From marine bands to hybrid flows: Sedimentology of a Mississippian black shale. Sedimentology, 67, pp261-304

Emmings, J.F., Hennissen, J.A., Stephenson, M.H., Poulton, S.W, Vane, C.H., Davies, S.J., Leng, M.J., Lamb, A., and Moss-Hayes, V., 2019. Controls on amorphous organic matter type and sulphurization in a Mississippian black shale. Review of Palaeobotany and Palynology, 268, pp. 1-18.

Emmings, J.F., Davies, S.J., Vane, C.H., Leng, M.J., Moss-Hayes, V., Stephenson, M.H. and Jenkin, G.R., 2017. Stream and slope weathering effects on organic-rich mudstone geochemistry and implications for hydrocarbon source rock assessment: A Bowland Shale case study. Chemical Geology, 471, pp.74-91.

Espitalié, J., Madec, M., Tissot, B., Mennig, J.J. and Leplat, P., 1977, May. Source rock characterization method for petroleum exploration. Offshore Technology Conference.

Espitalié, J., 1986. Use of Tmax as a maturation index for different types of organic matter: comparison with vitrinite reflectance. Collection colloques et séminaires-Institut français du pétrole, (44), pp.475-496.

Espitalié, J., Marquis, F. and Barsony, I., 1984. Geochemical logging. In Analytical pyrolysis (pp. 276-304). Butterworth-Heinemann.

Fraser, A. J., Gawthorpe, R. L., 2003. An Atlas of Carboniferous Basin Evolution in Northern England. Geological Society, London, Memoirs, 28.

Fraser, A.J. and Gawthorpe, R.L., 1990. Tectono-stratigraphic development and hydrocarbon habitat of the Carboniferous in northern England. Geological Society, London, Special Publications, 55(1), pp.49-86.

French, K.L., Tosca, N.J., Cao, C. and Summons, R.E., 2012. Diagenetic and detrital origin of moretane anomalies through the Permian–Triassic boundary. Geochimica et Cosmochimica Acta, 84, pp.104-125.

Gross, D., Sachsenhofer, R.F., Bechtel, A., Pytlak, L., Rupprecht, B. and Wegerer, E., 2015. Organic geochemistry of Mississippian shales (Bowland Shale Formation) in central Britain: Implications for depositional environment, source rock and gas shale potential. Marine and Petroleum Geology, 59, pp.1-21.

Harvey, H.R. and Mcmanus, G.B., 1991. Marine ciliates as a widespread source of tetrahymanol and hopan-3β-ol in sediments. Geochimica et Cosmochimica Acta, 55(11), pp.3387-3390.

Hennissen, J.A. and Montesi, G., 2020. Quantitative palynological analysis of the E2a and E2b goniatite biozones (Arnsbergian, Mississippian) in mudstones from the Southern Pennine Basin (UK). Review of Palaeobotany and Palynology, 276, p.104187.

Hennissen, J.A. and Gent, C.M., 2019. Total organic carbon in the Bowland-Hodder Unit of the southern Widmerpool Gulf: a discussion. Journal of Petroleum Science and Engineering, 178, pp.1194-1202.

Hennissen, J.A., Hough, E., Vane, C.H., Leng, M.J., Kemp, S.J. and Stephenson, M.H., 2017. The prospectivity of a potential shale gas play: An example from the southern Pennine Basin (central England, UK). Marine and Petroleum Geology, 86, pp.1047-1066.

Henry, D.G., Jarvis, I., Gillmore, G., Stephenson, M. and Emmings, J.F., 2018. Assessing low-maturity organic matter in shales using Raman spectroscopy: Effects of sample preparation and operating procedure. International Journal of Coal Geology, 191, pp.135-151.

Herrmann, J., Rybacki, E., Sone, H. and Dresen, G., 2018. Deformation experiments on Bowland and Posidonia Shale—part I: strength and Young's modulus at ambient and in situ pc–T conditions. Rock Mechanics and Rock Engineering, 51(12), pp.3645-3666.

Hu, M., Cheng, Z., Zhang, M., Liu, M., Song, L., Zhang, Y. and Li, J., 2014. Effect of calcite, kaolinite, gypsum, and montmorillonite on Huadian oil shale kerogen pyrolysis. Energy & fuels, 28(3), pp.1860-1867.

Isaksen, G.H. and Bohacs, K.M., 1995. Geological controls of source rock geochemistry through relative sea level; Triassic, Barents Sea. In Petroleum source rocks (pp. 25-50). Springer, Berlin.

Jarvie, D. M., 2012, Shale resource systems for oil and gas: Part 1— Shale-gas resource systems, in J. A. Breyer, ed., Shale reservoirs—Giant resources for the 21st century: AAPG Memoir, 97, pp.69–87

Jarvie, D.M., 1991. Total organic carbon (TOC) analysis: Chapter 11: Geochemical methods and exploration, in Merril, R. K., ed., Source and Migration processes and Evaluation Techniques: Treatise of petroleum geology, handbook of petroleum geology. Tulsa, Oklahoma, American Association of Petroleum Geologists, pp. 113-118.

Kirby, G.A., Baily, H., Chadwick, R.A., Evans, D.J., Holliday, D.W., Holloway, S., Hulbert, A.G., Pharaoh, T.C., Smith, N.J., Aitkenhead, N. and Birch, B., 2000. The structure and evolution of the Craven Basin and adjacent areas. Keyworth, Nottingham. British Geological Survey, pp.1-114.

Könitzer, S.F., Stephenson, M.H., Davies, S.J., Vane, C.H. and Leng, M.J., 2016. Significance of sedimentary organic matter input for shale gas generation potential of Mississippian Mudstones, Widmerpool Gulf, UK. Review of Palaeobotany and Palynology, 224, pp.146-168.

Könitzer, S.F., Davies, S.J., Stephenson, M.H. and Leng, M.J., 2014. Depositional controls on mudstone lithofacies in a basinal setting: implications for the delivery of sedimentary organic matter. Journal of Sedimentary Research, 84(3), pp.198-214.

Köster, J., Van Kaam-Peters, H.M., Koopmans, M.P., De Leeuw, J.W. and Damsté, J.S.S., 1997. Sulphurisation of homohopanoids: Effects on carbon number distribution, speciation, and 22S22R epimer ratios. Geochimica et Cosmochimica Acta, 61(12), pp.2431-2452.

Lafargue, E., Marquis, F. and Pillot, D., 1998. Rock-Eval 6 applications in hydrocarbon exploration, production, and soil contamination studies. Revue de l'institut français du pétrole, 53(4), pp.421-437.

Leeder, M.R., 1988. Recent developments in Carboniferous geology: a critical review with implications for the British Isles and NW Europe. Proceedings of the Geologists' Association, 99(2), pp.73-100.

Lodhia, B.H., Parent, A., Fraser, A.J., Nuemaier, M. and Hennissen, J. 2022. Thermal evolution and resources of the Bowland Basin (NW England) from apatite fission-track analyses and multidimensional basin modelling. In: Emmings, J., Parnell, J., Stephenson, M. and Lodhia, B. (eds) Processes and Resources in Fine-Grained Sedimentary Rocks: a Synthesis of Recent Research on a UK Mississippian Giant. Geological Society, London, Special Publications, in press.

Maynard, J.R., Hofmann, W., Dunay, R.E., Benthan, P.N., Dean, K.P. and Watson, I., 1997. The Carboniferous of Western Europe; the development of a petroleum system. Petroleum Geoscience, 3(2), pp.97-115.

McKirdy, D.M., Aldridge, A.K., Ypma, P.J.M., 1983. A geochemical comparison of some crude oils from pre-Ordovician carbonate rocks. In: Bjorøy, M. et al, 1981. Advances in Organic Geochemistry, John Wiley and Sons, New York, pp. 99-107.

Mews, K.S., Alhubail, M.M., and Barati, R.Gh., 2019. A Review of Brittleness Index Correlations for Unconventional Tight and Ultra-Tight Reservoirs. Geosciences, 9(7), pp. 319.

Moldowan, J.M., Peters, K.E., Carlson, R.M.K., Schoell, M. and ABUALI, M., 1994. Diverse applications of petroleum biomarker maturity parameters. Arabian Journal for Science and Engineering, 19(2 B), pp.273-298.

Moldowan, J.M., Sundararaman, P., Salvatori, T., Alajbeg, A., Gjukic, B., Lee, C.Y., and Demaison, G. J., 1992. Source correlation and maturity assessment of selected oils and rocks from the central Adriatic Basin (Italy and Yugoslavia), in J. M. Moldowan, J. M., P. Albrecht, and R. P. Philp, eds., Biological markers in sediments and petroleum: Englewood Cliffs, New Jersey, Prentice Hall, pp. 370–401.

Moldowan, J.M., Seifert, W.K. and Gallegos, E.J., 1985. Relationship between petroleum composition and depositional environment of petroleum source rocks. AAPG bulletin, 69(8), pp.1255-1268.

Morton, A., Waters, C., Fanning, M., Chisholm, I. and Brettle, M., 2015. Origin of Carboniferous sandstones fringing the northern margin of the Wales-Brabant Massif: Insights from detrital zircon ages. Geological Journal, 50(5), pp.553-574.

Newport, S.M., Hennissen, J.A., Armstrong, J.P., Taylor, K.G., Newport, L.P. and Hough, E., 2020. Can One-Run-Fixed-Arrhenius Kerogen Analysis Provide Comparable Organofacies Results to Detailed Palynological Analysis? A Case Study from a Prospective Mississippian Source Rock Reservoir (Bowland Shale, UK). Natural Resources Research, 29(3), pp.2011-2031.

Newport, S.M., Jerrett, R.M., Taylor, K.G., Hough, E., Worden, R.H., 2018. Sedimentology and microfacies of a mud-rich slope succession: in the Carboniferous Bowland Basin, NW England (UK). Journal of the Geological Society, 175(2), pp.147-262.

Peters, K.E., Burnham, A.K. and Walters, C.C., 2015. Petroleum generation kinetics: Single versus multiple heating-ramp open-system pyrolysis. AAPG Bulletin, 99(4), pp.591-616.

Peters, K.E., Walters, C.C. and Moldowan, J.M., 2005. The biomarker guide Volume 2. Second Edition. Cambridge university press, New York.

Peters, K.E. and Moldowan, J.M., 1991. Effects of source, thermal maturity, and biodegradation on the distribution and isomerization of homohopanes in petroleum. Organic geochemistry, 17(1), pp.47-61.

Peters, K.E., Moldowan, J.M. and Sundararaman, P., 1990. Effects of hydrous pyrolysis on biomarker thermal maturity parameters: Monterey phosphatic and siliceous members. Organic Geochemistry, 15(3), pp.249-265.

Peters, K.E., 1986. Guidelines for evaluating petroleum source rock using programmed pyrolysis. AAPG bulletin, 70(3), pp.318-329.

Quirk, M.M., Wardroper, A.M.K., Wheatley, R.E. and Maxwell, J.R., 1984. Extended hopanoids in peat environments. Chemical Geology, 42(1-4), pp.25-43.

Riley, N.J., 1990. Stratigraphy of the Worston Shale Group (Dinantian), Craven Basin, north-west England. Proceedings of the Yorkshire Geological Society, 48(2), pp.163-187.

Schwark, L. and Frimmel, A., 2004. Chemostratigraphy of the Posidonia Black Shale, SW-Germany: II. Assessment of extent and persistence of photic-zone anoxia using aryl isoprenoid distributions. Chemical Geology, 206(3-4), pp.231-248.

Sinninghe Damste, J. S., Kenig, F., Koopmans, M.P., Köster, J., Schouten, S., Hayes, J.M. and de Leeuw, J.W., 1995. Evidence for gammacerane as an indicator of water column stratification. Geochimica et Cosmochimica Acta, 59(9), pp.1895-1900.

Słowakiewicz, M., Tucker, M.E., Vane, C.H., Harding, R., Collins, A. and Pancost, R.D., 2015. Shale-gas potential of the mid-carboniferous bowland-hodder unit in the Cleveland basin (Yorkshire), central Britain. Journal of Petroleum Geology, 38(1), pp.59-75.

ten Haven, H.L., De Leeuw, J.W., Peakman, T.M. and Maxwell, J.R., 1986. Anomalies in steroid and hopanoid maturity indices. Geochimica et Cosmochimica Acta, 50(5), pp.853-855.

Timmerman, M.J., 2004. Timing, geodynamic setting and character of Permo-Carboniferous magmatism in the foreland of the Variscan Orogen, NW Europe. Geological Society, London, Special Publications, 223(1), pp.41-74.

Tyson, R.V. and Pearson, T.H. (eds), 1991. Modern and Ancient Continental Shelf Anoxia. Geological Society Special Publication, 58, pp.1-24.

Uemura, H. and Ishiwatari, R., 1995. Identification of unusual 17β (H)-moret-22 (29)-ene in lake sediments. Organic Geochemistry, 23(7), pp.675-680.

Volkman, J.K., 1986. A review of sterol markers for marine and terrigenous organic matter. Organic geochemistry, 9(2), pp.83-99.

Wang, C., 2007. Anomalous hopane distributions at the Permian–Triassic boundary, Meishan, China–evidence for the end-Permian marine ecosystem collapse. Organic Geochemistry, 38(1), pp.52-66.

Wang, T.G., Simoneit, B.R.T., Philp, R.P. and Yu, C.P., 1990. Extended 8. beta.(H)-drimane and 8, 14-secohopane series in a Chinese boghead coal. Energy & fuels, 4(2), pp.177-183.

Waples, D.W. and Machihara, T., 1990. Application of sterane and triterpane biomarkers in petroleum exploration. Bulletin of Canadian Petroleum Geology, 38(3), pp.357-380.

Waters, C.N., Holliday, D.W. and Chisholm, J.I., 2020a. The contribution of publications of the Yorkshire Geological Society to the understanding of the geological development of the Carboniferous Pennine Basin, northern England. Proceedings of the Yorkshire Geological Society, 63(1), pp.1-32.

Waters, C.N., Vane, C.H., Kemp, S.J., Haslam, R.B., Hough, E. and Moss-Hayes, V.L., 2020b. Lithological and chemostratigraphic discrimination of facies within the Bowland Shale Formation within the Craven and Edale basins, UK. Petroleum Geoscience, 26(2), pp.325-345.

Waters, C.N. and Condon, D.J., 2012. Nature and timing of Late Mississippian to Mid-Pennsylvanian glacio-eustatic sea-level changes of the Pennine Basin, UK. Journal of the Geological Society, 169(1), pp.37-51.

Waters, C.N., Waters, R.A., Barclay, W.J. and Davies, J.R., 2009. A lithostratigraphical framework for the Carboniferous successions of southern Great Britain (Onshore). British Geological Survey.

Whitelaw, P., Uguna, C.N., Stevens, L.A., Meredith, W., Snape, C.E., Vane, C.H., Moss-Hayes, V. and Carr, A.D., 2019. Shale gas reserve evaluation by laboratory pyrolysis and gas holding capacity consistent with field data. Nature communications, 10(1), pp.1-10.

Yang, S. and Horsfield, B., 2020. Critical review of the uncertainty of Tmax in revealing the thermal maturity of organic matter in sedimentary rocks. International Journal of Coal Geology, 225, p.103-500.

Yang, S., Horsfield, B., Mahlstedt, N., Stephenson, M. and Könitzer, S., 2016. On the primary and secondary petroleum generating characteristics of the Bowland Shale, northern England. Journal of the Geological Society, 173(2), pp.292-305.

Figure Captions

Figure 1. Shows oxic-anoxic levels as defined by Tyson and Pearson (1991) against the Eh values as well as oxygen and H_2S concentrations (Algeo and Li 2020). For reference the sulphidic zones identified by Emmings et al (2020) have been included to relate observations from trace element composition with organic biomarkers. Ratios of palaeoredox indicative biomarkers have been included after Peters et al (2005) demonstrating expected levels for each of the zones.

Figure 2. A) Map of the location of northern England boreholes in relation to the structural basin framework of the Carboniferous seaways of northern England. Basins of northern England mapped after Fraser and Gawthorpe (1990), updated after Andrews (2013) and Lodhia, et al. (2023). Well names are shortened as follows CH = Croft House, CS3 = Cominco-S3, MHD4 = Marl Hill Moor MHD4, WY = Wray. B) Core panels from Croft House, Wray, Cominco-S3 and Marl Hill Moor MHD4. TOC content is reported as wt.%, HI is reported in mg HC/g TOC, OI is mg CO_2/g TOC and Tmax is reported in °C. Cores have been positioned stratigraphically, solid red and dashed pink lines refer to identified biostratigraphic zonation as described in the text. Relative sea levels interpreted from Waters and Condon (2012). The lithological key is the same as for Figure 3. C) Common plots for interpreting organic matter type and maturity from programmed pyrolysis datasets. Literature zones describing calcareous and marine facies are from Newport et al (2018) and Emmings et al 2020 showing the majority of samples analysed align with published trends, in particular with argillaceous facies.

Figure 3. A) Map of the location of sampled boreholes from the Central Pennines or East Midlands. Majority of samples were taken from within the Widmerpool Gulf Basin. Basins of northern England included for reference as in Figure 2. Boreholes abbreviated as follows: WM = Wardlow Mires-2, CDRC4 = Carsington Dam Reconstruction-C4, IE = Ipstones Edge, LF = Lees Farm and RMP = Rempstone-1. B) Core panels from the aforementioned boreholes positioned stratigraphically. TOC content is reported as wt.%, HI is reported in mg HC/g TOC, OI is mg CO_2/g TOC and Tmax is reported in °C. solid red and dashed pink lines refer to identified biostratigraphic zonation as described in the text. Relative sea levels interpreted from Waters and Condon (2012). C) Plots for interpreting organic matter type and maturity from programmed pyrolysis datasets showing the range within the Central Pennine Dataset. Overall hydrocarbon generation potential interpreted from these plots is greater for this region.

Figure 4. A) Biplots of biomarker indices. i. is of Pristane/n-C_{17} over Phytane/n-C_{18} with organic matter type and depositional lines overlain, showing predominantly mixed kerogen type. ii. Is a ternary plot of sterane abundances based on the peak areas of the C_{27-29} $\alpha\alpha\alpha R$ steranes. iii. Plot of Gammacerane Index (GI) over Pr/Ph. Majority of data points cluster in the saline dysoxic zone. B) biomarker log plots for Pendleian-Brigantian aged samples from across northern England showing relative trends in biomarker ratios. Carbon Preference Index (CPI) is interpreted after the Bray and Evans (1961) method.

Figure 5. A) Biplots of biomarker indices. i. is of Pristane/n-C_{17} over Phytane/n-C_{18} with organic matter type and depositional lines overlain, showing a similarly predominantly mixed kerogen type. ii. Is a ternary plot of sterane abundances drawn as in Figure 4 using the C_{27-29} $\alpha\alpha\alpha R$ steranes to eliminate diasterane effects. iii. Plot of Gammacerane Index (GI) over Pr/Ph. Data clusters in the saline dysoxic zone as in Figure 4Aiii however this dataset has more samples representing oxic saline conditions. B) Logs of biomarkers in comparison to stratigraphy for the Ansbergian age sampling sites from the current study. CPI is interpreted as in Figure 4B.

Figure 6. GC-MS-SIM 191.1 plots of select samples from the dataset showing different distributions of terpanes. Labels are at the correct times for each chromatogram, and the numbers correspond to compounds listed in Table 1

Figure 7. GC-MS-SIM 217 and relevant EIC's showing the C_{27-29} sterane content. The m/z 217 EIC is labelled with regular sterane peaks that clearly coeluted with diasteranes. The 259 EIC is labelled to show key diasterane peaks (D). m/z 372-400 EIC's labelled with identified diasteranes found in the samples. Labels correspond to compounds in Table 1.

Figure 8. EIC of m/z 133 showing the distribution of aryl isoprenoids. m/z 134 EIC was used to identify peaks, as the 133 EIC shows a range of additional unidentified aromatic compound peaks. Compounds are denoted by their carbon number, as Cn.

Figure 9. Mineral ternary diagram after Hennissen et al (2017), showing the distribution of Mississippian samples against mudstone classifications. Two groups of mudstone type were found, the first was highly argillaceous comprised almost entirely of clay and silicate minerals. The second group is a more siliceous mudstone. Average areas for US Shale Plays after Mews, et al (2019) and references therein is also displayed, this showed comparison between siliceous UK Carboniferous mudstones and the Barnett Formation suggesting locations such as Lees Farm-1 and Marl Hill Moor MHD4 more suitable as a classic shale play.

Figure 10. Cross plot of Pr/Ph over AIR. Trend has a positive correlation, after Schwark and Frimmel (2004) this indicated that samples towards the axis intercept have persistent reducing conditions in the photic zone. Samples with relatively higher Pr/Ph and AIR have more episodic conditions. Samples have been sorted by the facies type from Figures 2-5 to highlight trends from the relative environmental conditions of deposition. Two groups were identified, Group 1 relates to marine type facies i.e. carbonate slope, marine bands and hemipelagite which demonstrate enhanced reducing deposition. Group 2 primarily consists of the turbidite facies which would be deposited under episodic conditions.

Figure 11. Different crossplots of common biomarker maturity indices against Tmax recorded from programmed pyrolysis. A) Hopane isomers. B) Moretane ratio, calculated from hopane values as $30b\alpha/(30b\alpha+30ab)$. C) Ts/(Ts+Tm) the red arrow shows the anticipated maturity trend for this biomarker.

Figure 12. A) Plot of Ts/Tm versus C27 diasterane ratio, approximate maturity trend would be positive and linear which is represented by the red arrow. The effect of oxidation produces an orthogonal trend to maturity demonstrated by samples with a low Ts/Tm and higher Diasterane ratio. B) Diasteranes versus Tmax shows that as Tmax increases so do rearranged steranes, which would normally by indicative of maturation. However, the boreholes have such a range of Tmax values over short periods that a mineral matrix effect is deduced to have created such a trend. C) show the ratios of hopane isomers for C_{31} homohopanes against the diasterane ratio. The linear trend is indicative that controls on Tmax and diasterane distribution also effect the ratio of hopane isomers demonstrating the significance of mineral matrix effects. D) Correlates diasteranes to percent abundance of clay minerals identified through XRD analysis, a positive relationship was found which indicates a connection between clay deposition and organic preservation or alteration. Turbidite facies samples have the highest diasterane ratio and clay mineral contents, while hemipelagic facies has the lowest of both. Interestingly, marine band facies shows variability and thus other chemical effects might be the cause of the relationship.

Table Captions

Table 1. List of biomarkers and acronyms used for organic constituents found in this study.

Number Assigned	Compound Name	Acronym	Compound Class	Carbon Number
1	22,29,30-Trisnorneohopane	Ts	Trisnorhopane	27
2	22,29,30-Trisnorhopane	Tm	Trisnorhopane	27
3	17a(H)-Diahopane	$C_{29}*$	Diahopane	29
4	17a-norhopane	$C_{28}Nor$	Norhopane	28
5	17a,21b(H)-30Norhopane	$29\alpha b$	Norhopane	29
6	18a(H)-30-norneohopane	29Ts	Norneohopane	29
7	17a(H)-Diahopane	$C_{30}*$	Diahopane	30
8	17b,21a(H)-30Norhopane (normoretane)	$29b\alpha$	Moretane	29
9	17a,21b(H)-Hopane	H / $30\alpha b$	Hopanes	30
10	17a(H)-30-Nor-29-Homohopane	30Ts	Norneohopane	30
11	17b21a(H)-hopane (moretane)	$30b\alpha$	Moretane	30
12S	17a,21b(H)-29-Homohopane 22S	$C_{31}S$	Homohopanes	31
12R	17a,21b(H)-29-Homohopane 22R	$C_{31}R$	Homohopanes	31
13	Gammacerane	G	N/A	30
14S	17a,21b(H)-29-Homohopane 22S	$C_{32}S$	Homohopanes	32
14R	17a,21b(H)-29-Homohopane 22R	$C_{32}R$	Homohopanes	32
15S	17a,21b(H)-29-Homohopane 22S	$C_{33}S$	Homohopanes	33
15R	17a,21b(H)-29-Homohopane 22R	$C_{33}R$	Homohopanes	33
16S	17a,21b(H)-29-Homohopane 22S	$C_{34}S$	Homohopanes	34
16R	17a,21b(H)-29-Homohopane 22R	$C_{34}R$	Homohopanes	34
17S	17a,21b(H)-29-Homohopane 22S	$C_{35}S$	Homohopanes	35
17R	17a,21b(H)-29-Homohopane 22R	$C_{35}R$	Homohopanes	35
18	5α(H),13α(H),17α(H)-Cholestane (S)	$27\alpha\alpha\alpha S$	Regular Steranes	27
19	5α(H),13β(H),17β(H)-Cholestane (S+R)	$27\alpha bb R + 27\alpha bb S$	Regular Steranes	27
20	5α(H),13α(H),17α(H)-Cholestane (R)	$27\alpha\alpha\alpha R$	Regular Steranes	27
21	5a(H),14a(H),17a(H) methylcholestane (S)	$28\alpha\alpha\alpha S$	Regular Steranes	28
22	5a(H),14b(H),17b(H) methylcholestane (S+R)	$28\alpha bb R + 28\alpha bb S$	Regular Steranes	28
23	5a(H),14a(H),17a(H) methylcholestane (R)	$28\alpha\alpha\alpha R$	Regular Steranes	28
34	5a(H),14a(H),17a(H) ethylcholestane (S)	$29\alpha\alpha\alpha S$	Regular Steranes	29
25	5a(H),14b(H),17b(H) ethylcholestane (S+R)	$29\alpha bb R + 29\alpha bb S$	Regular Steranes	29
26	5a(H),14a(H),17a(H) ethylcholestane (R)	$29\alpha\alpha\alpha R$	Regular Steranes	29

27	13b,17a(H)-Diacholestane (S)	27*baS*	Diasteranes	27
28	13b,17a(H)-Diacholestane (R)	27*baR*	Diasteranes	27
29	13a,17b(H)-Diacholestane (S)	27*abS*	Diasteranes	27
30	13a,17b(H)-Diacholestane (R)	27*abR*	Diasteranes	27
31	13b,17a(H)-Diacholestane (S)	28*baS*	Diasteranes	28
32	13b,17a(H)-Diacholestane (R)	28*baR*	Diasteranes	28
33	13a,17b(H)-Diacholestane (S)	28*abS*	Diasteranes	28
34	13a,17b(H)-Diacholestane (R)	28*abR*	Diasteranes	28
35	13b,17a(H)-Diacholestane (S)	29*baS*	Diasteranes	29
36	13b,17a(H)-Diacholestane (R)	29b*a*R	Diasteranes	29
37	13a,17b(H)-Diacholestane (R)	29*a*bR	Diasteranes	29

Table 1
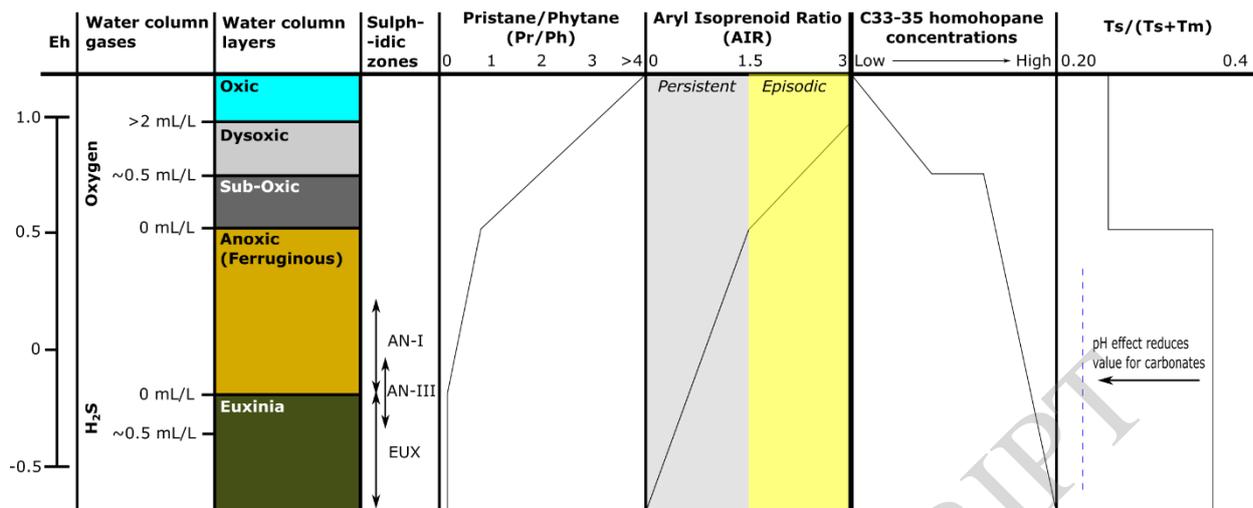
Figure 1
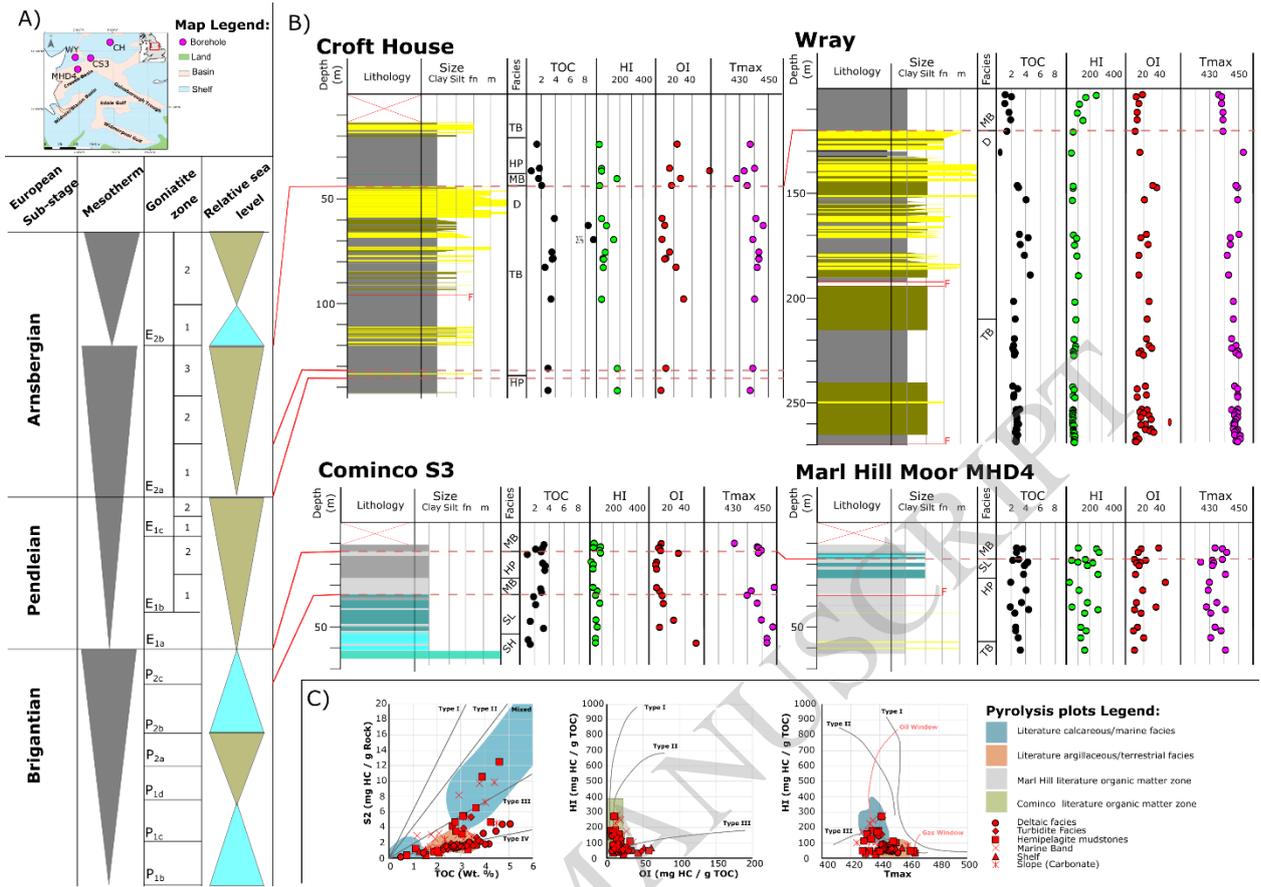
Figure 2
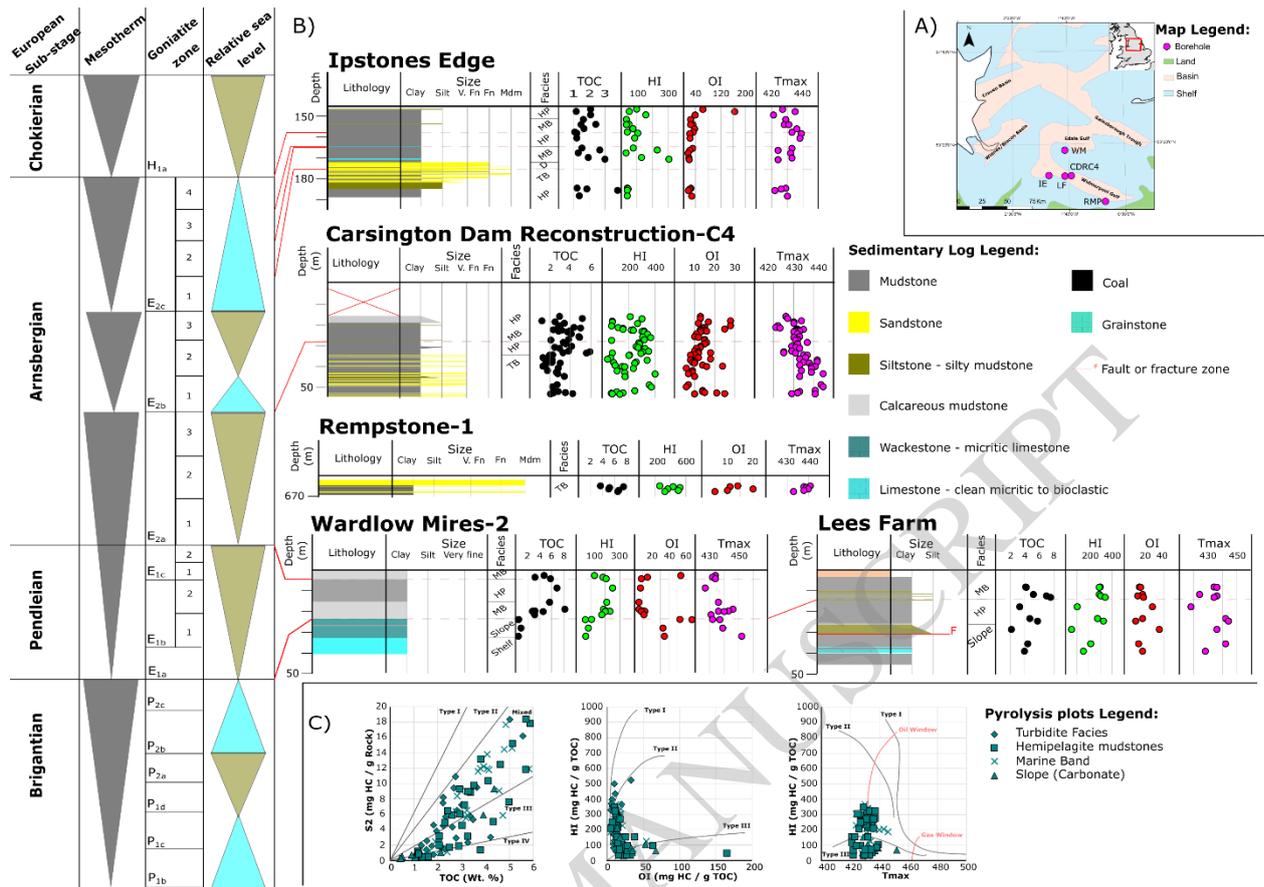
Figure 3
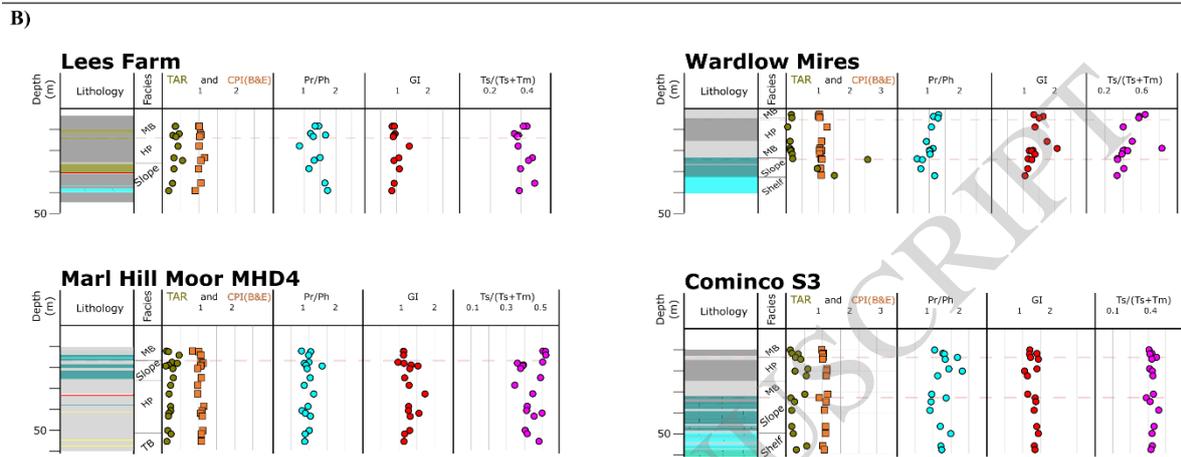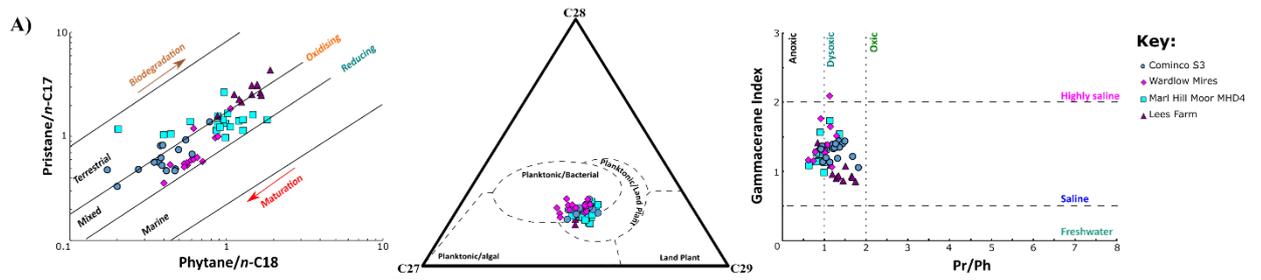
Figure 4
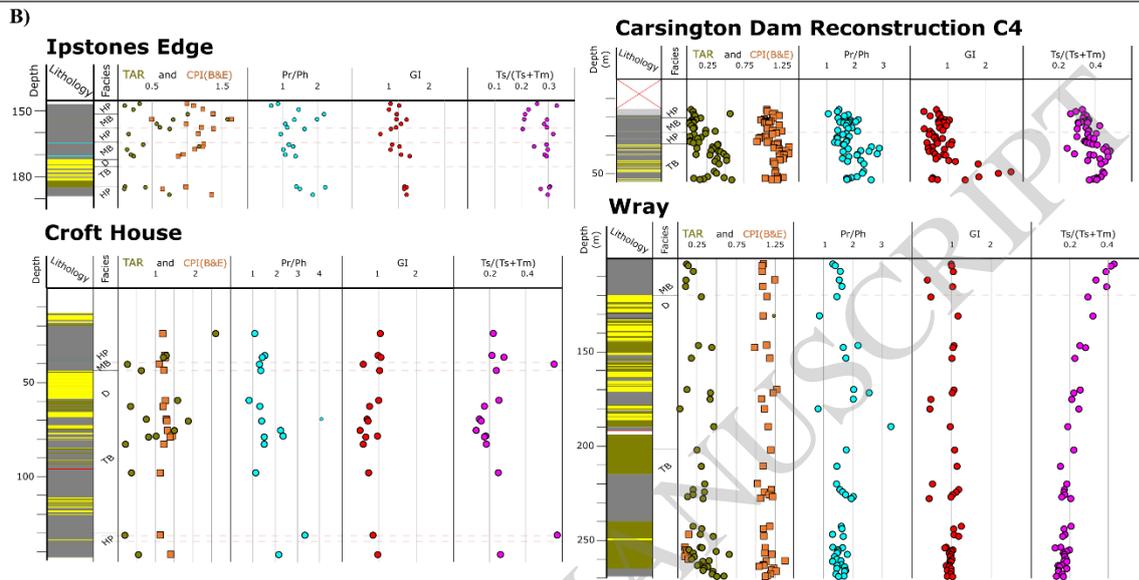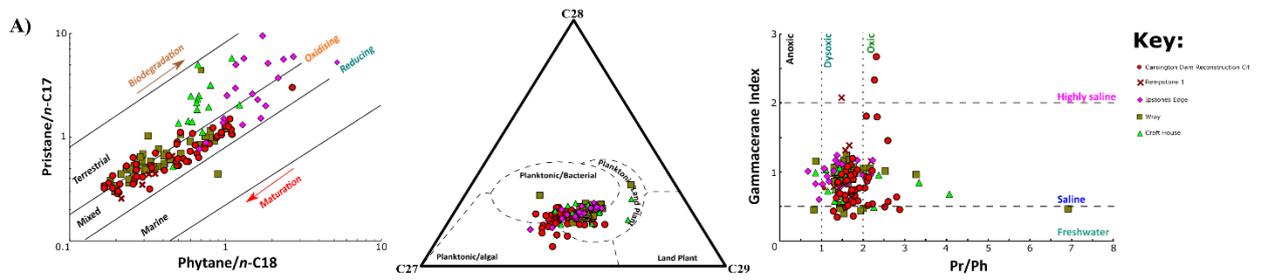
Figure 5
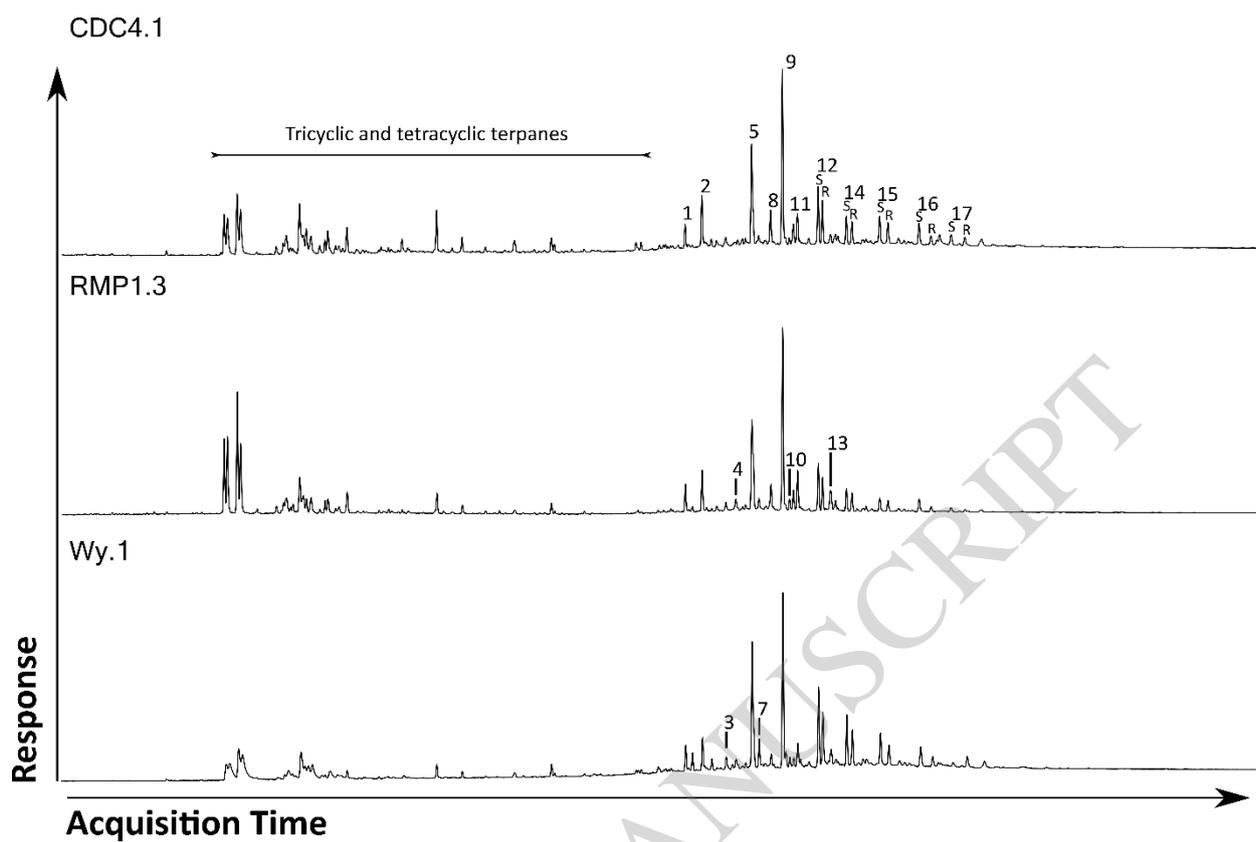
Figure 6

Figure 7

Figure 8

Carbonates

Calcareous
Mudstone

Eagle Ford

*Ductile
- Brittle
Transition
Zone*

Mudstone

Siliceous
Marlstone

Marcellus

Bakken

Argillaceous
Mudstone

Siliceous
Mudstone

Barnett

Clay

Silicates

□ Marl Hill Moor MHD4
▲ Lees Farm
● Carsington Dam
   Reconstruction C4
✖ Rempstone 1
■ Wray
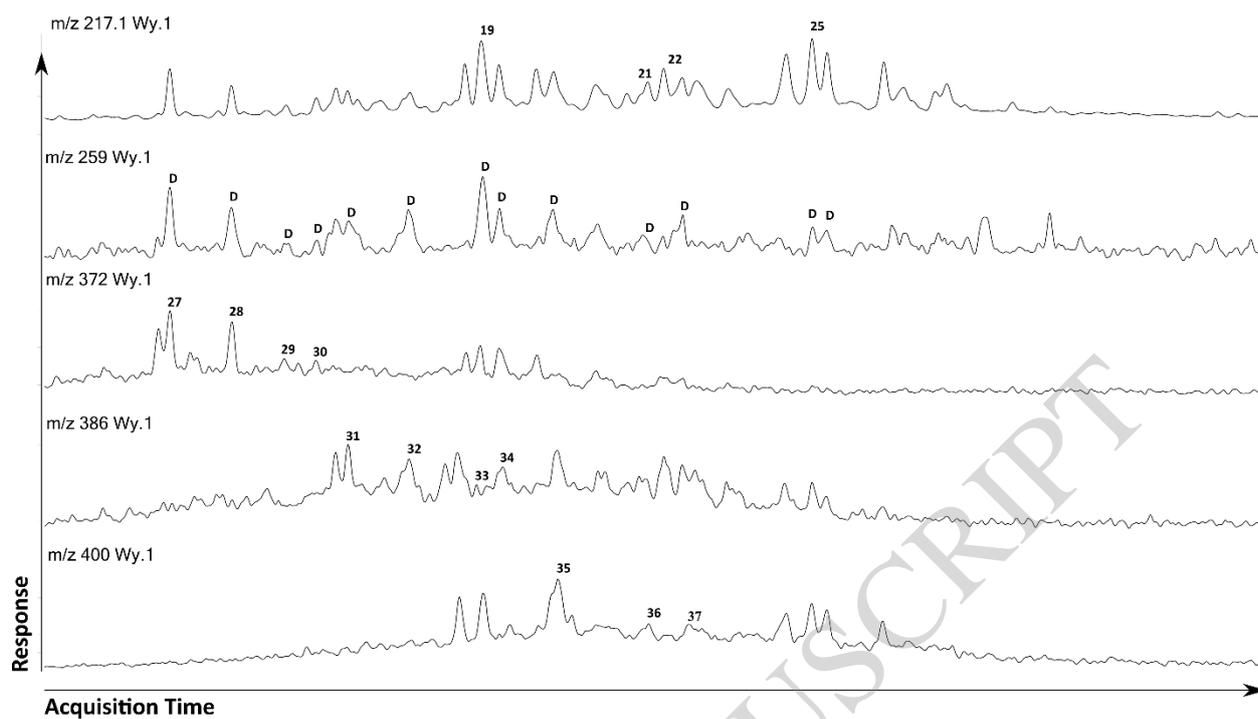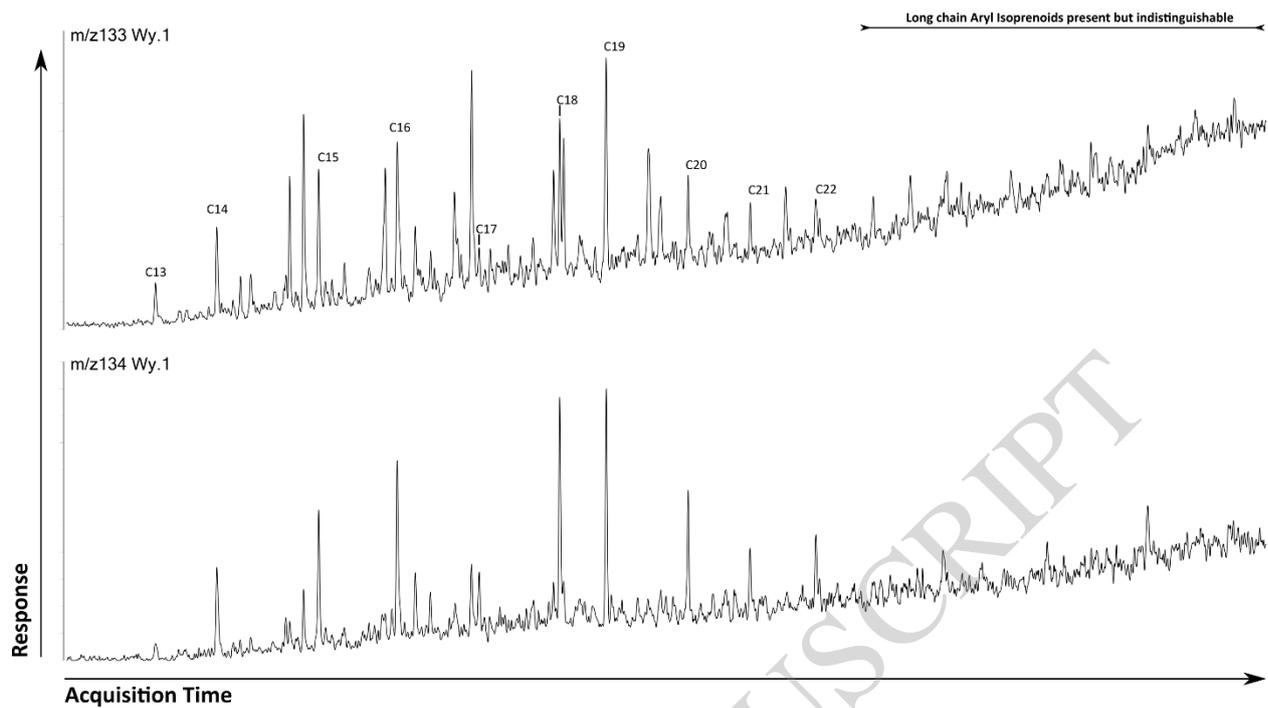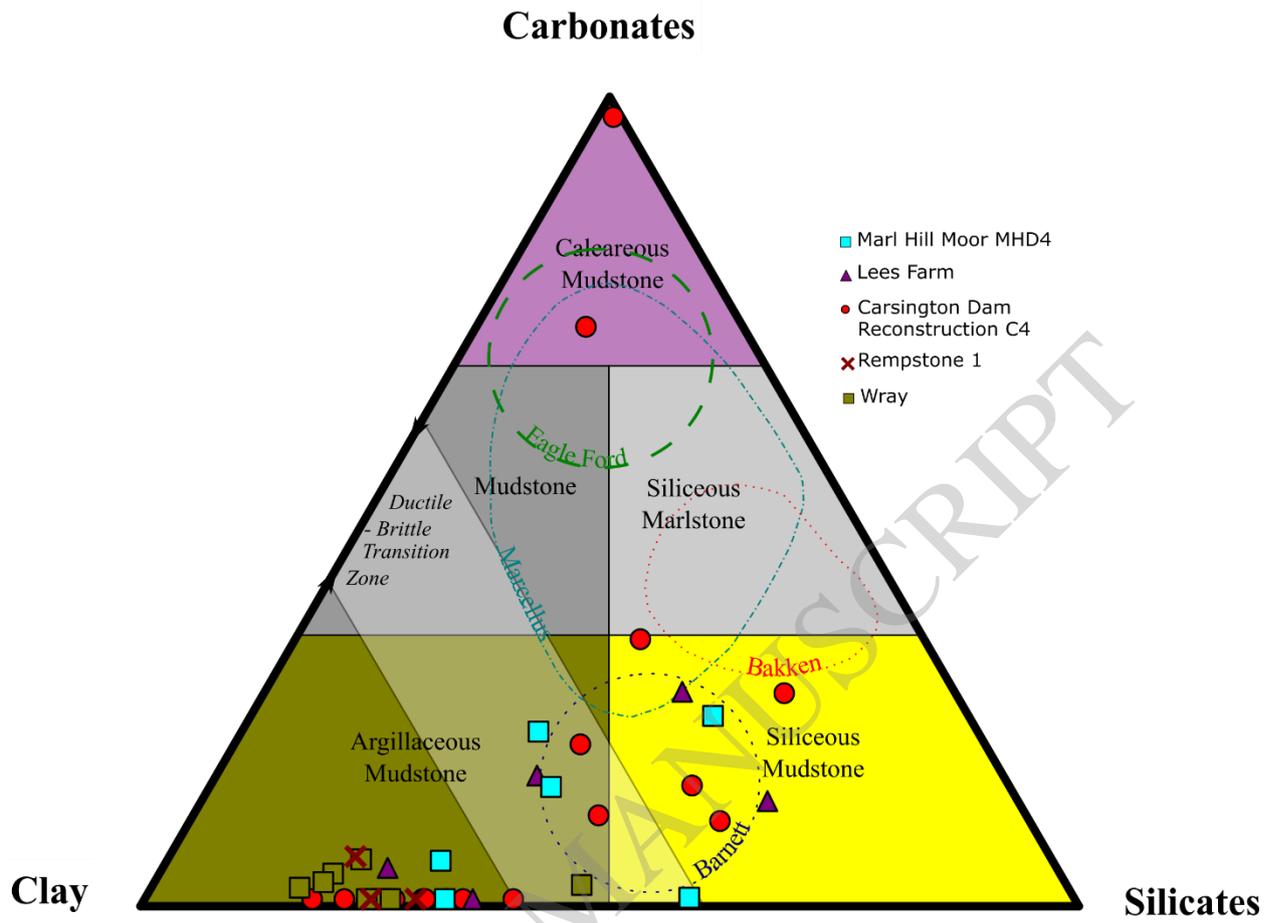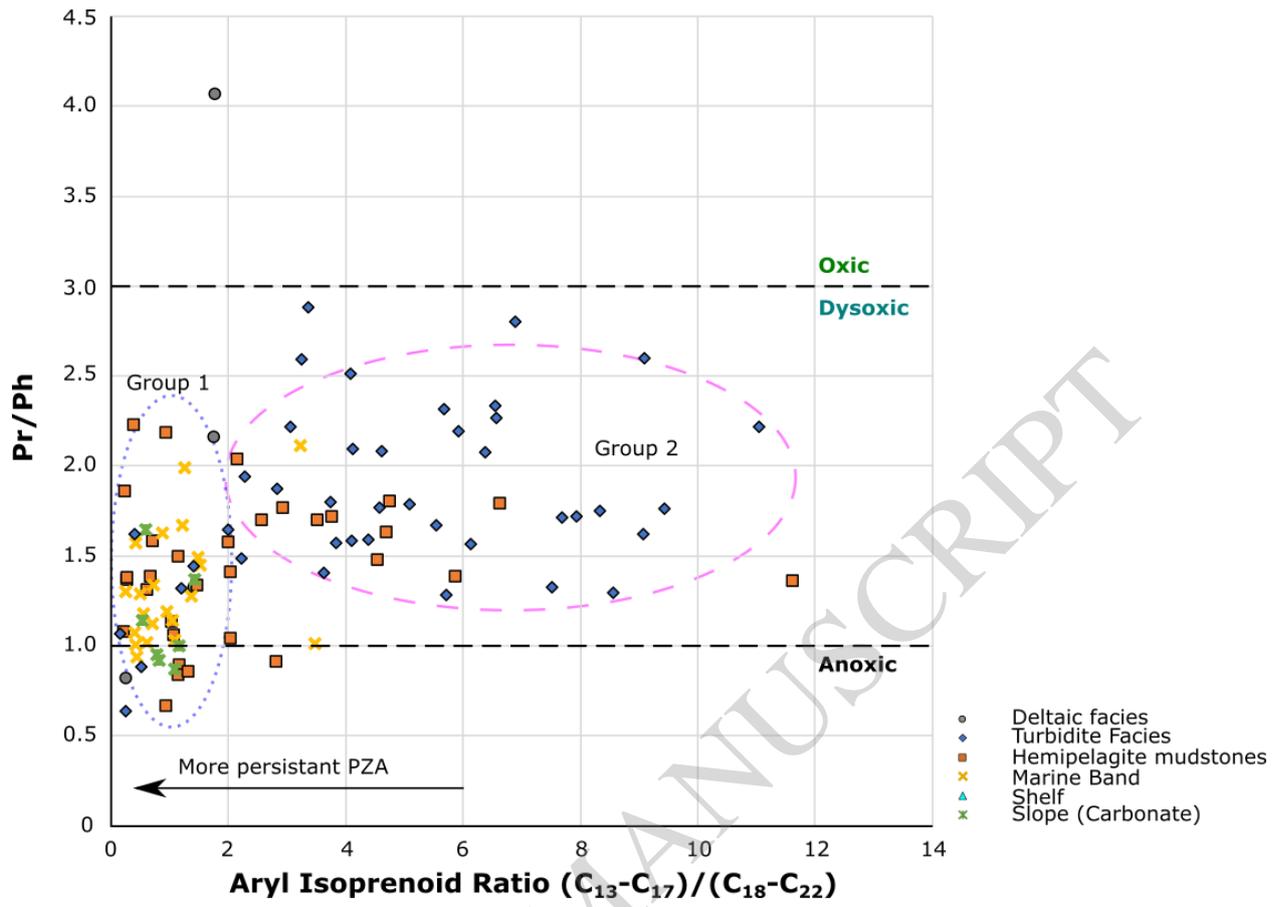
Figure 9

Figure 10

Figure 11

Figure 12